Recent progress in 2D layered III-VI semiconductors and their heterostructures for optoelectronic device applications

*Zhibin Yang, Jianhua Hao**

Dr. Z. Yang

Center for Terahertz Waves and College of Precision Instrument and Optoelectronics Engineering, and the Key Laboratory of Optoelectronics Information and Technology, Ministry of Education, Tianjin University, Tianjin 300072, P. R. China

Dr. Z. Yang, Prof. J. Hao

Department of Applied Physics, The Hong Kong Polytechnic University, Kowloon, Hong Kong, P. R. China

Email: jh.hao@polyu.edu.hk

Keywords: layered III-VI semiconductors, optoelectronic devices, broadband photodetectors, photovoltaic devices, 2D heterostructures

Abstract

During the past decade, great research efforts have been devoted to two-dimensional (2D) layered materials due to their reduced thickness and extraordinary physical properties, which opens new opportunities for developing next-generation applications in various fields. In the 2D family, ultrathin III-VI semiconductors (e.g., GaSe, InSe, In_2Se_3 etc.) have emerged as potential candidates for nano-optoelectronic applications thanks to their sizable layer-dependent band gaps and high carrier mobility, which could enable broadband photodetection and efficient conversion of solar energy. Here, we aim to provide a

systematic review on the 2D III-VI semiconductors based state-of-the-art optoelectronic devices, such as phototransistors, photoconductors, solar cells ~~and so on ,~~ reported in recent years. To better understanding the mechanism and performance of the devices, the review starts with an introduction on the electronic structures and optical properties of several representative III-VI members. Then a comprehensive overview is given on the design of device geometries, operating principles and performances of optoelectronic applications based on III-VI semiconductors as well as their heterostructures. The techniques to enhance the performances of devices are also discussed. Finally, we conclude the review with a brief discussion on the challenges and future opportunities in this field.

1. Introduction

The stacks of atomically thin layered materials have become one of the most exciting fields in nowadays materials science.[1,2] The so-called two-dimensional (2D) layered materials not only share many excellent properties from their bulk counterparts, but also show some unique physical characteristics owing to the quantum confinement effect.[3,4] Majority of bulk form of 2D materials consists of atomically thin layers with weak van der Waals (vdWs) interlayer connections, which allow them to be separated by scotch tape or liquid-phase exfoliation.[5–7] The ease fabrication method makes the portfolio of 2D family expanding rapidly in the past decade. Apart from semi-metallic graphene, numerous semiconducting 2D materials have been discovered up to now, such as the group of transition metal dichalcogenides (TMDs), ultrathin black phosphorus (BP), silicene ~~and so on~~, which could ideally address the drawback of zero band gap of graphene.[8–12] In contrast

to the usual three-dimensional (3D) bulk semiconductors, 2D layered semiconductors have shown specific advantages for modern real device applications, such as atomic-scale thickness, free of dangling bonds, good flexibility, atomic smoothness et al..[13,14] Particularly, the development of optoelectronic devices based on 2D semiconductors and their heterostructures is a rapidly expanding field thanks to their fascinating optical properties, with appreciable bandgaps covering from ultraviolet (UV) to infrared (IR) region.[15][16] For example, a typical member of TMDs, 2D MoS_2 based photodetector has shown a large photoresponsivity of 880 A/W, and well-defined electroluminescence (EL) spectra have been observed from the vertical heterostructure of WSe_2/MoS_2, revealing important potential for photo-sensing and light-emitting diode (LED) applications.[17,18]

Similar to TMDs, III-VI layered materials are another significant group of 2D semiconductors, which has gain renewed interests for optoelectronic applications in recent years thanks to their tunable bandgaps, efficient light absorption, and large carrier mobility.[19,20] In general, based on different stoichiometric, layered III-VI materials can be divided into two main subgroups, which are MX (e.g., GaSe,[21] GaTe,[22] InSe[23] et al.), and M_aX_b (e.g., In_2Se_3,[24] In_2S_3,[25] In_3Se_4[26] et al.), exhibiting different crystalline and electronic structure. Differing from MoS_2, III-VI layered semiconductors usually show a number of distinct polymorphs, such as α-, β-, γ- for InSe, making the group covering a wide range of characteristics.[27] Particularly, the optical bandgap of III-VI layered semiconductors ranges from 1.25 (IR) to 3.05 eV (UV) (**Table 1**), showing a large optical window in 2D limit, which makes them potential candidates for different functional optoelectronic devices, such as light-emitting diodes (LEDs), phototransistors and solar cells (**Figure 1**).[28,29] One typical example of III-VI semiconductors is 2D layered InSe,

exhibiting amazing electronic transport properties (electron mobility ≈ 1055 $cm^2V^{-1}s^{-1}$) and broadband photodetection from UV to near infrared (NIR) attributing to its narrow and tunable band gaps, which are much superior to those of MoS_2.[30–32] Meanwhile, extremely high photoresponsivity of around 10^4 A/W and ultrafast response speed (~120 μs) can be obtained in InSe photodetectors, which greatly satisfy the demand for future optoelectronics.

More recently, 2D vdWs heterostructures have drawn significant research attention since they can be simply formed by stacking or stitching the atomically thin layers in either vertical or lateral way, respectively, which may provide new opportunities to realize fascinating phenomena by combining those materials with different characteristics.[33–35] In general, 2D heterostructures based on III-VI semiconductors usually exhibit type-II band alignment, which could boost the separation efficiency of electron-hole pairs for optoelectronic applications.[36,37] Meanwhile, the built-in potential at the interface of 2D heterojunction allows the self-driven photodetection ability.[37] So far, most of the recent review articles on III-VI semiconductors provide a comprehensive overview on the synthesis, properties and applications of the family.[19,20] However, a specific review on the optoelectronic devices based on 2D III-VI members has not been given yet although this topic is covered by many original research articles in recent years. In this review, we systematically summarize the recent efforts and progress on the development of photo-sensing and light-harvesting devices based on several typical III-VI semiconductors and their heterostructures. Initially, the crystal structure and optical properties of different polytypes of III-VI layered materials will be briefly introduced. Then we will review the performance and mechanisms of the photodetectors and solar cells based on a variety of

III-VI semiconductors and their artificial heterostructures. Several techniques to optimize the device performance are also discussed. Finally, the review is summarized with some perspectives and potential research directions in the field are provided.

2. Geometric and optical properties of group III-VI semiconductors

The target applications of materials are mainly dominated by their crystal structure and physical properties. Therefore, it is essential to introduce the geometric and electronic structure of 2D III-VI semiconductors as well as their optical properties firstly for better understanding their potential in nano-optoelectronics. In general, the crystal structure of monolayer III-VI semiconductor is constructed by two vertically stacked layers of IIIA metal ions sandwiched between two layers of chalcogenides, which are connected by vdWs forces (**Figure 2**a). The variations in the sequence of stacks result in different polytypes of III-VI materials. In this section, the structural and optical properties of III-VI group will be demonstrated by analyzing 2D GaSe and InSe, which are two representative members of this group.

Bulk GaSe has a direct band gap of ~2 eV and exhibits a p-type semiconducting behavior.[38,39] Generally, GaSe crystals possess four different polytypes (β-, ε-, γ-, δ-), which show different electronic and optical properties.[39] Among them, β-GaSe has an inversion symmetric center, exhibiting the space group of D^4_{6h}. On the other hand, according to the side and top-view of ε-GaSe unit cell (Figure 2a), ε-GaSe shows a 2H stacking and non-centrosymmetric structure, which makes it desirable for applications of nonlinear optics. Recently, our group and other group observed the second-harmonic

generation (SHG) effect in both few- and mono- layer of GaSe nanosheets [38,40], providing a new platform to study the non-resonance feature of the 2D layered materials.

According to the previous theoretical calculation, a layer-dependent electronic band structure of 2D GaSe is predicted.[39] According to Figure 2b, the valence band maximum (VBM) of ε-GaSe symmetrically splits up relative to the Γ point when the layer number is smaller than 7, revealing that the transition to indirect band gap occurs for ultrathin GaSe nanosheets. Meanwhile, the band gaps of 2D GaSe (<7 layer) shows increasing trend along with decreasing of layer number due to the quantum confinement effect as demonstrated in Figure 2c. This varying trend of band gaps is consistent with the experimental results, which exhibits blue-shift of photoluminescence emission from the exfoliated GaSe nanosheets.[21] The intriguing band gap crossover from direct-to-indirect for ultrathin nanosheets is in contrast to that of 2D MoS_2, which exhibits an indirect-to-direct band gap transition for monolayer sample.[41]

Besides GaSe, InSe is another typical layered III-VI semiconductor, which possesses a graphene-like honeycomb lattice with each layer consisting of close-packed Se-In-In-Se sheets (Figure 2d).[27,42] Based on the arrangement of stacking sequence, there are four different polytypes of layered InSe (β-, ε-, γ-, and δ-).[20] Among them, β- and γ- are two most studied phases of 2D InSe, where primitive unit cell of β-InSe composes of two covalently bonded monatomic layers. For γ-InSe, there are three quaternary layers in one unit cell, where In atoms in one layer align with Se atoms in another layer, leading to the breaking of mirror-plane symmetry (Figure 2d).[42] Earlier studies have shown that bulk InSe possessing a direct band gap of ~1.25 eV and anisotropic electronic properties at room temperature.[29] However, when the thickness is smaller than a threshold value, the band

gap of 2D InSe nanosheets shows a crossover transition from direct to indirect which is similar to that of 2D GaSe.[43] As shown in Figure 2e, the VBM position moves gradually from Λ point to Γ point along with increasing of layer number, which can be explained by the interlayer coupling of lone electron pairs between neighboring monatomic layers. According to the experimental results, such threshold thickness is around 6 nm.[23] Interestingly, although ultrathin InSe owns an indirect band gap, strong light absorption can still be observed due to the assistance of phonons (inset of Figure 2e). Figure 2f presents the theoretically thickness-dependent electronic band diagram for different thick InSe, exhibiting band gaps decreasing from 2.12 eV (monolayer) to 1.08 eV (five-layer), which is consistent with the previously reported photoluminescence emission results.[29,42,44] Such a wide range of band gaps from visible to near-infrared region makes 2D InSe desirable for developing high performance optoelectronic devices.

3. III-VI semiconductor based optoelectronic devices

There are two main categories of III-VI semiconductors based on the stoichiometric composition: MX (e.g. GaS, GaSe, GaTe, InS, InSe), and M_aX_b (e.g. Ga_2Se_3, In_2Se_3, In_3Se_4). In this section, the optoelectronic devices based on gallium monochalcogenides, indium monochalcogenides and In_2Se_3 will be illustrated in sequence, respectively.

3.1 Gallium chalcogenide based photosensing devices

In this sub-section, we will review photo-sensing devices based on 2D layered gallium chalcogenides, such as GaSe, GaS and GaTe.

3.1.1 GaSe photodetectors

GaSe is one of the typical layered III-VI semiconducting materials, which has been widely used in nonlinear optics applications, terahertz wave detection and optoelectronic devices. Crystalline bulk GaSe has a hexagonal layered structure with each layer constructed by covalent bonds in the sequence of Se-Ga-Ga-Se. In general, bulk GaSe crystal is a p-type semiconductor with an indirect band gap of around 2.11 eV, which is 0.025 eV less than the value of direct band gap.[21,45] Compared with the bulk counterparts, the ultrathin 2D GaSe possesses a tunable band gap and good photoresponse performance due to the quantum confinement effect. Up to now, the atomically thin GaSe nanosheets have been realized by various techniques, including mechanical cleavage methods,[21,46] vapor phase mass transport methods[45] and pulsed laser deposition (PLD).[47]

Due to its outstanding optical properties and good thermal stability (≤ 600 ^{o}C), the ultrathin GaSe nanosheets obtained by mechanical exfoliation have been fabricated into nanoscale photodetectors.[21] The optoelectronic properties of the device were studied under illumination of a monochromatic light with wavelength of 254–610 nm (**Figure 3**a). The GaSe based photodetector exhibits a large photoresponsivity of 2.8 A/W, external quantum efficiency (EQE) of 1367 % and fast response speed (~20 ms). In addition, another primary figure-of-merit of photodetector, linear dynamic range (LDR), which describes the range of linear photoresponse of the photodetector, was extracted from the curve of photocurrent versus the illumination intensity as shown in Figure 3b. LDR is significant for evaluating the performance of photodetectors since the light signal beyond the range cannot be detected or calculated accurately. For GaSe based photodetector, the obtained LDR is 32.8 dB in response to a 500 W halogen lamp, which is limited by the

relatively small photocurrent. Apart from the rigid substrate, 2D GaSe photodetectors have also been demonstrated on flexible transparent substrates (Figure 3c).[48] The GaSe nanosheets were grown on mica substrates by a catalyst-free vdWs epitaxy method. As shown in Figure 3d, a stable dynamic photoresponse of the device was observed, exhibiting a large photocurrent on/off ratio of around 110. Meanwhile, GaSe/mica photodetector showed good durability since considerable photoresponse can be observed after repeated bending process.

2D layered materials have been considered as a promising candidate for gas sensing applications due to their high surface-to-volume ratio, which could provide large active area to interact with gas molecules.[49–51] Recently, Yang et al. demonstrated tuning of photoresponses of few-layer GaSe nanosheets based phototransistors in different gas environment. The device was characterized under a 254 nm UV light in either O_2 or air as shown in Figure 3e. The sensitivity of the GaSe phototransistor was also optimized by a thermal annealing process, providing more selenium vacancies in the GaSe nanosheets. Interestingly, in comparison with the as-exfoliated ones, the annealed samples shows larger photoresponsivity (18.75 A/W), fast response speed and high photocurrent on/off ratio (~150) in the O_2 circumstance as shown in Figure 3f. Here, O_2 molecules acts as an acceptor, which could increases the hole carrier density of p-type GaSe nanosheets. The thermal annealing process can effectively increase the charge transfer between O_2 and GaSe, which would improve the sensitivity of the phototransistor.

Piezo-phototronics coined by Zhong Lin Wang is one of the emerging fields in flexible electronics and optoelectronics, which optimizes the optoelectronic performance of the devices by applying a mechanical stimuli.[52–54] In recent years, piezo-phototronic effect

has been observed in several 2D layered materials with piezoelectric properties, such as MoS_2, enabling the development of novel nano opto-electro-mechanical devices.[55,56] More recently, 2D materials of group-III monochalcogenides were predicted piezoelectric in their monolayer form by first-principles calculations.[57] Experimentally, Jia et al. firstly reported the observation of strong piezo-phototronic effect in 2D GaSe based photodetector due to its remarkable semiconducting and optical properties and attractive piezoelectric feature.[58,59] **Figure 4**a presents the schematic drawing of setup for studying the strain effect on the performance of GaSe photodetector. The initial wrinkle providing strain can be clearly identified in atomic force microscopy (AFM) image as shown in the inset of Figure 4b. With an increase in mechanical strain, the photocurrent generated was enhanced accordingly and showed a linear increasing trend for strain larger than 0.1 % (Figure 4b), indicating that the mechanical stimuli has strong influence on the optoelectronic properties of GaSe nanosheets. The photoresponse is mainly determined by the distribution of the strain in the wrinkle. According to Figure 4c, the current of device under illumination is rapidly reduced when the strain slightly decreases, and then saturated with further decreasing the strain for different applied biases. The mechanism of the piezo-phototronic effect was illustrated by the band diagram of GaSe as a function of strain (Figure 4d). The band gap modulation induced by strain will produce a local electric field, which will provoke carriers concentrating at the surface of the wrinkles. As shown in Figure 4d, two conductive layers appear due to the built-in field, resulting in enhancement for the photoresponse of the device. The robust durability of the GaSe flexible device was tested by repeated manually bending process under illumination (Figure 4e). Under more than 20 bending cycles, a stable enhancement of the current can be observed, revealing robust

suitability of the piezo-phototronic effect and good flexibility of GaSe nanosheets. Overall, 2D layered GaSe is expected to be a potential candidate for nano-optoelectronic devices and flexible opto-electro-mechanical applications.

3.1.2 Other gallium chalcogenides

Regarding the group of 2D layered III-VI semiconductors, GaS possesses largest optical band gap of around 3.05 eV, which makes it a potential candidate for near-blue optoelectronic applications.[28] In recent years, a series of photo-sensing devices have been developed based on ultrathin GaS nanosheets, which are realized by mechanical exfoliation method. The first example of optoelectronic device based on GaS nanosheet was reported by Hu et al., demonstrating ultraviolet (UV) to visible GaS photodetector on rigid substrate (SiO_2/Si) and flexible substrate (polyethylene terephthalate (PET)) (**Figure 5**a), respectively.[28] Devices made on both substrates exhibit strong wavelength dependent photoresponses. According to Figure 5b, the photoresponsivity and detectivity of the flexible device show distinct decreasing trend when increasing the illumination wavelength. It is noteworthy that the responsivity of the photodetector at 254 nm is about 20 times higher than that of the device at 550 nm, revealing good photodetection ability for UV region of the GaS based photodetectors, which results from the large band gap of GaS nanosheets. Meanwhile, the peak responsivity value (~19.2 A/W) of the flexible device is much larger than those of typical 2D materials, such as graphene, monolayer MoS_2, and it is about fourfold over the performance of GaS based photodetectors on rigid substrate. The possible reason is that the photocurrent in GaS nanosheets could be weakened by the hydroxyl groups or any other defects at the interface of SiO_2. Furthermore, the response

time of GaS based flexible photodetectors has not been influenced by the mechanical deformation of the device, indicating good stability of their photodetection ability.

Similar to GaSe, 2D GaS nanosheets is also sensitive to the surrounding gaseous environment. Recently, Yang et al. investigates the performance of GaS based photodetectors in different gas circumstances (air, O_2 and NH_3).[60] As shown in Figure 5c, the time-dependent photoresponse measurement exhibits that the photocurrent and current switching ratio of devices in NH_3 are much higher than those of devices in air or O_2 environment. The enhancement of photoresponse of the device in NH_3 is owing to an increase in carrier density of GaS nanosheets by the adsorption of NH_3 molecules, which act as the donor to transfer electrons into GaS.

Among 2D layered gallium chalcogenides, GaTe is the only one with natural direct band gap, which makes it promising for optoelectronic applications.[61] Differing from InSe, 2D GaTe does not undergo a direct-to-indirect band gap transition at ultrathin thickness. Liu et al. have investigated the optoelectronic properties of few-layer GaTe based photodetectors (Figure 5d).[22] According to Figure 5e, the photoresponsivity measured at drain bias of 5 V shows a linear decreasing trend relative to the light intensity, which may result from the trap states and defects either in the layer or the interface of GaTe nanosheets. The maximum responsivity obtained is as high as 10^4 A/W, which is several orders higher than those from some other 2D materials, such as graphene, MoS_2 and BP. In addition, the response time of GaTe photodetector is less than 20 ms, and could be tuned by the gate biases, revealing promising response speed for photo sensing. In addition to rigid substrate, flexible GaTe photodetectors have also been fabricated by transferring the CVD grown GaTe nanosheets on PET substrates.[62] After eliminating the surface adsorbates in an

ultrahigh vacuum, the flexible GaTe photodetector shows fast response time of 54 ms and excellent stability of photoresponse. More recently, Wang et al. reported that the Ga vacancy defects also have strong influences on the electronic and optoelectronic performance of GaTe based phototransistors.[63] The characterization of phototransistors was carried out in vacuum at liquid nitrogen temperature, which will effectively suppress the Ga ion vacancies. The obtained photogain and responsivity are 2000 and 800 A/W, respectively, which exhibit comparable performance to those of MoS_2 based devices. At the same time, the suppression of Ga vacancies will largely improve the response speed of the phototransistor as shown in Figure 5f, which decreases from 11.5 s (ambient) to 0.3 s (vaccum and low temperature). Overall, direct band gap and good electrical properties suggest 2D GaTe to be integrated into photo sensing devices with high photoresponsivity and fast response speed.

3.2 Indium monochalcogenides based photosensing devices

Apart from gallium chalcogenides, indium monochalcogenides is another main group of 2D layered III-VI semiconductors. Typical materials of indium monochalcogenides, such as InSe and InS, usually exhibit several distinct polytypes with different crystal structures and large, tunable band gaps. In this section, optoelectronic devices, including photodetectors and solar cells, based on InSe and InS nanosheets will be introduced, respectively.

3.2.1 InSe photodetectors

In contrast to gallium chalcogenides, 2D layered InSe exhibits narrower band gaps, which makes it more sensitive to visible and NIR spectrum.[27,64] In addition, smaller exciton

reduced mass makes InSe undergoing stronger quantum confinement effect than other III-VI members, resulting in good controllability on the band gaps by the layer number.[23,27,29] Rapid advances in preparing high quality mono- and few-layer InSe nanosheets by mechanical exfoliation,[23,31] liquid-based exfoliation,[65] PLD,[44] chemical vapor deposition (CVD)[66] et al., have paved the way for developing nano-optoelectronic devices. For instance, Tamalampudi et al. have demonstrated high performance photodetectors based on mechanical exfoliated few-layer InSe on both rigid and flexible substrates.[31] As shown in **Figure 6**a, the InSe photodetector on SiO_2/Si substrates was characterized by using a back gate configuration, exhibiting a broadband photodetection ability from 450 nm (visible) to 785 nm (NIR). Under illumination of 633 laser, the device showed a maximum photoresponsivity of 7 A/W, and achieved a detectivity as high as $\sim 1.07\times10^{11}$ Jones, which is much superior to the performance of MoS_2 based photodetectors.[67,68] Furthermore, the gate bias dependence of photoresponse was studied under illumination (λ = 633 nm, V_{ds} = 10 V). According to Figure 6b, the photoresponsivity at V_g = 70 V is 157 A/W, which is more than three orders of magnitude higher than that at V_g = -60 V. Such good controllability of photoresponsivity by gate bias is meaningful for the pixelated imaging applications.[31] In addition, the optoelectronic properties of flexible InSe photodetector on PET substrates were also investigated (Inset of Figure 6c), exhibiting excellent stability and reproducibility thanks to the stretchable feature of ultrathin InSe nanosheets.[31] As shown in Figure 6c, the photocurrent recorded in planar state increases along with the incident light intensity, which is similar to the behavior of device on rigid substrate. The obtained detectivities of flexible photodetector in the bent and unbent states

are 4.58×10^{10} and 5.47×10^{10} Jones, respectively, which are comparable to the performance of the device on SiO_2/Si.

Wafer-scale synthesis technique for 2D layered materials is urgently desired for realizing practical applications.[69–73] Recently, our group has demonstrated phototransistors based on centimeter-scale highly crystalline InSe thin films (Inset of Figure 6d).[44] Under illumination of light source with different wavelength, the InSe phototransistors show a broadband photoresponse from 370 nm (UV) to 980 nm (NIR) (Figure 6d). The recorded peak values of photoresponsivity and EQE are as high as 27 A/W and 9000 %, respectively, which are several orders higher than those of graphene and MoS_2 based devices measured under similar conditions.[44] The high responsivity could be explained by high absorption of InSe nanosheets due to the direct band gap and the photogating effect.

Self-powered devices are significant for some emergency situations but without external power supply. Recently, Li et al. demonstrated a photoelectrochemical (PEC)-type self-powered photodetector based on solution exfoliated InSe nanosheets.[74] The optoelectronic measurements were conducted in 0.2 M KOH electrolyte under the irradiation of simulated sunlight (Figure 6e). The photocurrent density obtained without any external power sources was 15.9 nA/cm^2, confirming self-powered feature of the device. Moreover, the InSe PEC-photodetector also showed good cycle and time stability and almost maintained steady performance over 50 cycles and 24 hours, respectively. In this work, the KOH electrolyte not only improves the stability of the ultrathin InSe nanosheets, but also effectively modulates the performance of photodetection. As shown in Figure 6f, the photocurrent can be well controlled by both the external bias voltage and concentration of KOH. With increasing the KOH concentration, the photoresponse of the device exhibits stronger

dependence on the bias voltage. Furthermore, under zero bias potential, the photocurrent density changes dramatically from 0.03 to 15.6 nA/cm^2 when the KOH concentration increases from 0.05 to 0.2 M, revealing good controllability of concentration of electrolyte on the performance of PEC-photodetector.

3.2.2 Enhanced InSe photodetectors

Owing to the ultrathin thickness of 2D materials, the light absorption of 2D layer is very low, making it challenging to develop a broadband photodetector with high detectivity based on merely pristine 2D samples. To address the issue, several strategies have been exploited to enhance the performance of 2D optoelectronic devices.[75–77] Among them, plasmonic technique has been proved to be able to enhance the photoresponse of 2D layered materials effectively by improving the photoelectric conversion efficiency, which benefits from the optimized light-harvesting ability and high near-field induced by the plasmonic effect.[78,79] Recently, Dai et al. have designed a dual-band self-powered photodetector based on hybrid structure of mechanical exfoliated InSe nanosheets and Au plasmonic nanoparticles (NPs).[80] The triangular Au NPs arranged in hexagonal pattern were placed on top of InSe based Schottky diode, which was constructed by fabricating electrodes with asymmetric metals (**Figure 7**a). Compared with pristine InSe photodetectors, the InSe/Au device extends the photodetection spectral range from UV-vis to UV-vis-NIR (350–950 nm). Meanwhile, InSe/Au photodetector exhibits an enhancement of photoresponsivity with high wavelength selectivity due to the quadrupole plasmons of Au NPs. In particular, the responsivity of InSe/Au at the wavelength of 685 nm is about 12 times higher than that of InSe device. LDR of the devices was measured under zero bias voltage, exhibiting largely enhancement from 43 to 64 dB at the wavelength

of 650 nm, which is similar to that of photodetectors based on InGaAs. Detectivity is another significant figure-of-merit for characterizing the performance of photodetection. In this work, within the spectral from UV to NIR, the detectivity of InSe/Au is always larger than that of pristine InSe photodetector as shown in Figure 7b. The maximum enhancement ratio of detectivity appears at the wavelength of 685 nm as well, which increases from 2.56×10^{11} to 3.35×10^{12} Jones, revealing an excellent upgrade of 2D InSe photodetectors.

Besides surface plasmonic based technique, another strategy called surface oxidation doping (SOD) has also been utilized to enhance the performance of photodetectors based on 2D InSe nanosheets.[81] An uniform and smooth oxidation layer was produced on top of InSe nanosheets by indirect incident oxygen plasma, which could effectively control the level of surface oxidation. Benefiting from the SOD effect, the oxidation layer could modulate the distribution gradient of the charge carrier concentration, creating a vertically built-in electrical field, which largely enhance the separation efficiency of the photoexcited electron-hole pairs under illumination. As shown in Figure 7c, the photoresponsivity of InSe photodetector shows strongly dependence on both wavelength of incident light and the oxidation degree of SOD process. Within a broadband spectral range from UV (365 nm) to NIR (850 nm), the photoresponsivity increases with the level of oxidation until the treatment time at 10 s, and then decreases with further increasing the oxidation degree. It is because the concentration of photo-carriers are augmented by the SOD effect, but the carrier transport mobility declines at higher degree of oxidation. Under the optimized oxidation condition, the obtained photoresponsivities of InSe photodetectors are as high as 5×10^6 A/W and 5×10^5 A/W at 365 nm and 530 nm, respectively, which exhibits

extremely high enhancement compared with photodetectors based on pristine InSe.[27,29,44,82]

Previous reports mainly focus on enhancing the photoresponsivity of InSe photodetectors, but the research on optimization of response speed is rare. A fast photoresponse is significant for the applications of telecommunications, photodetection, high-speed imaging et al.. Recently, Lei et al. have made use of avalanche effect to optimize the performance of ultrathin InSe based nanosheets, which exhibits remarkable improvement of photoresponse performance of InSe device from all sides.[83] Patterned Al electrodes were fabricated to form large Schottky barriers with InSe layer, which enables the appearance of avalanche effect by a large external bias voltage (inset of Figure 7d). Figure 7d presents the photoresponse of InSe avalanche photodetector under different intensity of incident light. It is worth noting that the curves of photocurrent versus bias voltage can be divided into three parts. The avalanche effect is triggered at the external biases in the range from 12 to 50 V, leading to noticeably increasing of photocurrent. The working principle is that the amount of carrier multiplication increases with the bias voltage, making high photogain of the device (Figure 7e). The obtained EQE at 50 V bias is as large as 344 % under illumination intensity of 8.8 mW/cm^2. Meanwhile, the dark current of the device is largely suppressed owing to the large reverse-biased Schottky barrier, exhibiting a mildly increasing trend with bias potential in the avalanche effect region. When the bias voltage is larger than 50 V, the dark current is significantly enhanced due to the breakdown of the reverse bias, which would decrease the magnitude of signal-to-noise (S/N) ratio. Therefore, the voltage interval of appearance of avalanche effect would be the optimized condition to achieve better photodetection performance. Besides the high quantum

efficiency, the obtained response time of the InSe avalanche photodetector is 60 μs, which is approximately 3 orders faster than the normal InSe photosensing devices.[31,84] To further optimize the performance of the device, an array of plasmonic Al nanodisks was fabricated on top of InSe photodetector, which could improve the light absorption of InSe nanosheets as we discussed previously. Functioned by both avalanche effect and surface plasmonic technique, the photocurrent of the device was dramatically enhanced (Figure 7f). Under the conditions of 30 V bias voltage and light intensity of 44 mW/cm^2, the optimized device exhibits an EQE as high as 866 % and short response time of 87 μs, revealing an overall enhancement to the performance of ordinary InSe photodetectors.

3.2.3 InSe based Schottky solar cell

Thanks to the direct band gaps and strong light-matter interaction, InSe microplates have been fabricated into a solar cell with Schottky-type configuration.[82] As shown in **Figure 8**a, the surface photovoltage (SPV) measurement was constructed by transferring the ε-InSe microplate on top of copper substrate, which acted as the bottom electrode. An In-coated mesh on top of InSe served for the top electrode. The incident light with the photon energy ranged from 0.65 to 3.5 eV was applied to characterize the surface photovoltaic effect of the InSe solar cell. As shown in Figure 8b, three distinct peaks can be observed in the photovoltaic response spectrum, which may result from the surface recombination induced by the relatively low surface barrier of In-InSe. These three peaks A (0.85 – 1.05 eV), B (1.1 – 1.25 eV), C (1.75 – 2.5 eV) here could be induced by the surface trap states at the interface, the band edge transition of free exciton, and transition of E_1, respectively. The results reveal that the In-InSe solar cell generally converts the photon energy from 1 eV, which is desirable for the photoelectric conversion of sunlight. A simulated sunlight

source with white light emission was employed to characterize the photoelectric properties of the In-InSe Schottky solar cell as shown in Figure 8c. The obtained output photovoltage was around 24 mV under an average illumination intensity of 0.83 mW/cm^2, exhibiting observable photoelectric conversion behavior (Figure 8d).

3.2.4 InS phototransistor

Besides InSe, ultrathin layered InS is another typical 2D indium monochalcogenides, which has been studied insufficiently from both physical properties and device applications.[85,86] In general, the stable phase of InS possesses an orthorhombic structure assembled in a network architecture, which exhibits the optical indirect band gap of around 1.78 eV, making it a potential candidate for photonic and optoelectronic devices ranging from red light to NIR region. Recent work demonstrated a photo-metal-semiconductor-field-effect transistor (Photo-MESFET) based on strip-like InS nanosheets (inset image of **Figure 9**a).[85] The photoconductivity measurement was carried out under illumination of either a tungsten halogen (W) lamp or a white-light LED. As shown in Figure 9a, the *I-V* characteristics of InS device exhibit that the photoresponse of W lamp is significantly higher than that of white-light LED, because the radiation peak of W lamp (~1.8 eV) is more close to the band gap of InS (~1.78 eV). Particularly, the obtained photoresistivity ratio for the device illuminated by W lamp and LED is around 86 % and 30 %, respectively (Inset curve of Figure 9a). Furthermore, the performance of InS Photo-MESFET has been characterized by measuring the relationship between I_d and V_g under different drain biases (Figure 9b). The transconductance g_m has been extracted to be around 0.272 ± 0.005 μA/V for the illumination of W lamp with intensity of ~3 mW/cm^2. The g_m of InS phototransistor is smaller than that of InSe device due to the indirect band gap.[87] Further investigation

could be conducted to optimize the performance of InS phototransistors according our previous discussion.

3.3 In_2X_3 (X = S, Se, Te) based optoelectronic devices

Apart from indium monochalcogenides, In_2X_3 (X = S, Se, Te) is another intriguing group of 2D layered III-VI family, which has already found a series of proof-of-concept applications, such as photodetectors, solar cell, memory devices ~~and so on~~, benefiting from their direct band gap, high efficiency of light absorption, large carrier transport mobility and ferroelectricity.[88–90] In this sub-section, photoconductors/phototransistors based on In_2S_3 and In_2Se_3 are reviewed and discussed.

In general, crystalline In_2Se_3 possesses five different crystallographic phases (α, β, γ, δ, κ), where only α- and β-In_2Se_3 exhibit vdWs layered structure with stacking of atomically thin sheets in the sequence of Se-In-Se-In-Se.[88,91,92] Previous report presents that the layered α-In_2Se_3 has a thickness dependent optical band gap across a broad range from 1.45 eV (bulk) to 2.8 eV (thin flake) due to the strong quantum confinement effect, making it attractive for high performance photosensors in near-UV to NIR region.[88] Up to now, the ultrathin In_2Se_3 nanosheets have been realized by various techniques, including mechanical exfoliation, CVD, vdWs epitaxy and physical vapor deposition (PVD).[89,93,94] The fabrication method used is crucial to the performance of the nano-optoelectronic devices based on 2D In_2Se_3.

Recently, photodetectors based on mechanical exfoliated α-In_2Se_3 nanosheets have been demonstrated, exhibiting extremely large photoresponsivity and detectivity in a broadband spectral region.[95] The patterned platinum was used as electrodes, while TiN was deposited to pad the trenches in SiO_2, resulting in a uniform contact with the In_2Se_3 nanosheet (**Figure**

10a). A monochrome light source was used to conduct the photoresponse measurement in the spectral range of 300 –550 nm. The extracted photoresponsivity could reach as high as 3.95×10^3 A/W and 59 A/W at 300 nm and 500 nm, respectively, which are much superior to those of GaS, GaSe, InSe based photodetection applications.[21,28,31] Meanwhile, the EQE and detectivity, the other two significant figures-or-merit of photodetectors, have also been calculated based on the magnitude of responsivity. As shown in Figure 10b, both EQE and detectivity of the device show a decreasing trend with an increase in the wavelength of incident light. It is worth noting that the In_2Se_3 exhibit ultrahigh EQE of 1.65×10^5 % and detectivity of 2.26×10^{12} Jones at wavelength of 300 nm, respectively, revealing desirable performance for sensitive photodetection applications in UV-vis-NIR region.

Apart from α-In_2Se_3, the layered β-In_2Se_3 has also been developed into photodetectors, exhibiting high photoresponsivity and fast response times as well.[96] Here, monolayer β-In_2Se_3 nanosheets have been prepared by a colloidal synthesis technique, resulting in the samples with lateral scale ranged from ~300 to ~900 nm. The processing temperature (~200 ^oC) is much lower than those of techniques for growing 2D In_2Se_3, such as PLD, vdWs epitaxy and physical vapor transport.[91,93,94] Previous studies indicate that bulk β-In_2Se_3 possesses a direct optical band gap of 1.3 eV,[97] but undergoing a transition to indirect band gap of around 1.55 eV when the thickness decreasing to monolayer.[96] The photodetector was constructed by dispersing the β-In_2Se_3 solution on SiO_2/Si substrate (Figure 10c). The measured response time is 2.5 ms for rise time and 3.7 ms for fall time, which are about one order faster than those of InSe and GaSe photodetectors.[21,31,44] Additionally, the dependence of photoresponsivity on photon energy shows a broadband photodetection from 1.6 eV to 3.3 eV, exhibiting an outstanding photoresponse upon the

whole visible region (Figure 10d). The maximum photoresponsivity can reach up to 7 × 10^4 A/W, which is even much higher than the photodetector based on mechanical exfoliated α-In_2Se_3.

The working principles of photodetectors based on 2D materials are usually functioned by a combination of several mechanisms, such as photovoltaic effect, photoconduction, photogating effect, photoelectric et al., which increases the difficulty to control the individual property of the device.[24,98,99] Recently, Island et al. demonstrated to fully modulate the performance of α-In_2Se_3 phototransistors by controlling the generation mechanism of photocurrent with back gate biases.[24] In their work, the contribution to the photocurrent from thermal mechanisms have been eliminated by a large laser spot, making the photocurrent mainly arising from the photoconductive and photogating effects. In general, the photocurrent induced by photoconductive effect shows a linear increasing relationship with the incident light intensity. On the other hand, the photogating generated current increases sub-linearly with the illumination intensity. Figure 10e demonstrates that the dominating mechanism of photocurrent generation changes from fast photoconduction at back gate bias of -40 V (OFF state) to high-gain photogating across the ON state. In the ON state, the photogain is strongly dependent on the gate voltage, showing an ultrahigh photoresponsivity up to around 1 × 10^5 A/W at back gate bias of 30 V under illumination of 640 nm laser, which is even superior to that of previously introduced β-In_2Se_3 photodetectors.[96] The enhancement of the photoresponse could be attributed to the oxide layer at surface and photogenerated holes trapped in long-lived states. Additionally, the detectivity of α-In_2Se_3 phototransistors can also be tuned by the back gate voltages in response to the illumination of 640 nm laser (Figure 10f). The obtained maximum

detectivity is as high as $(3.3 \pm 0.8) \times 10^{13}$ Jones at the gate bias of 20 V in the ON state, which is around three orders larger than that of InSe based photodetectors,[31] exhibiting great potential for high performance photodetection applications.

Among the family members of indium (III) chalcogenides, In_2S_3 is another attractive material for optoelectronic applications thanks to its large coefficient of light absorption, low toxicity and desirable photoelectric properties.[25] Similar to In_2Se_3, bulk In_2S_3 crystal also possesses several different crystalline phases (α, β, γ).[100] Among them, β-In_2S_3 exhibits a size-dependent direct optical band gap ranged from 1.9 to 2.3 eV at room temperature.[101] In addition, β-In_2S_3 crystal has intrinsic trap states, forming an intermediate band within the band structure, which gives rise to a series of interesting electronic and optoelectronic properties. Recently, CVD grown In_2S_3 nanosheets have been developed into photodetectors, exhibiting a broadband photodetection range from visible (400 nm) to NIR (1000 nm) region (Figure 10g).[25] The extracted photoresponsivity of In_2S_3 device can reach up to 137 A/W excited by illumination of 450 nm, which has notable superiority on the other III-VI layered semiconductors, such as pristine InSe nanosheets (12.3 A/W),[31] GaS (4.2 A/W)[28] and GaSe (2.8 A/W).[21] Moreover, the photocurrent of the device shows a linear relationship to the incident light intensity as shown in Figure 10h, exhibiting typical behavior of excellent photoconductive performance. The linear response can be explained by the presence of intrinsic trap states, which could arouse more photocarriers by absorbing extra energy of the excited electrons/holes.

4. Optoelectronic applications based on 2D group III-VI heterostructures

Most of the individual 2D layered materials suffer from some certain limitations for practical applications. For example, graphene possesses great electrical transport properties but lack of band gap, while phosphorene exhibits both large tunable band gaps and mobility but showing terrible stability in ambient. Thus, constructing ultrathin 2D heterostructures with combination of different 2D material features would display some new functionality and broaden the applications of 2D family.[35,102,103] For instance, 2D p-n heterojunction can be developed based on 2D semiconductors, providing a built-in potential in the depletion region, which could promote the separation of photogenerated electron-hole pairs and realizing efficient conversion of energy.[104] In the previous section, we mainly focus on the optoelectronic applications based on single III-VI semiconductors. In this section, the optoelectronic devices created by heterostructures based on 2D III-VI layered materials (GaSe, GaTe, InSe and In_2Se_3) will be demonstrated, including both vertically stacked and laterally jointed configurations.

4.1 Gallium chalcogenides based heterostructures

Based on the overview of recent works, in this sub-section, the optoelectronic devices, including photodetectors, phototransistors and solar cells constructed by 2D layered gallium chalcogenides (GaSe and GaTe) based heterostructures will be introduced.

4.1.1 GaSe heterostructures

According to our previous introduction, p-type layered GaSe is one of the compelling 2D materials for optoelectronic device applications.[21,45,48] So far, there have been several reports of 2D heterostructures based on GaSe, including GaSe/graphene, GaSe/MoS_2,

$GaSe/MoSe_2$, $GaSe/WS_2$, $GaSe/WSe_2$, exhibiting attractive photoelectric properties and proof-of-concept optoelectronic devices.[105–111] Among them, graphene has extremely high transport mobility and already demonstrated ultrahigh gain photodetectors by forming heterostructures with other 2D materials,[112,113] attributed to the formation of high quality interface due to the similar vdWs layered structure. It is worth noting that the quality of interface in 2D heterostructure plays a crucial role in the performance of devices. For instance, the low-resistance electrical contact can only be formed with strong interfacial interactions. In addition, the surface contamination should be eliminated to realize clean 2D interface. Recently, Lu et al. demonstrated a graphene/GaSe photodetector with a clean interface resulted from a vacuum annealing process, which could effectively reduce the interfacial deep trap states.[107] The device was fabricated by transferring the liquid exfoliated GaSe nanosheets on CVD grown graphene film (**Figure 11**a). The measured response time around 10 ms has been optimized by the vacuum annealing process, which is largely superior to that of the graphene/MoS_2 device (Figure 11b).[113] Meanwhile, an ultrahigh photogain around 1.28×10^7 was obtained at incident light intensity of 198 mW/cm^2. Both fast and high gain photoresponse makes graphene/GaSe heterostructures suitable for photodetection applications in visible light region.

As 2D GaSe is a p-type semiconductor, it is intriguing to create atomically thin p-n junction based on GaSe and another n-type 2D semiconductors, such as MoS_2, WS_2, $MoSe_2$ et al., which is propitious for the optoelectronic applications due to the efficient separation of electron-hole pairs induced the built-in electric field. One recent work demonstrated a heterojunction photodiode based on mechanical exfoliated GaSe and MoS_2 nanosheets with asymmetric electrical contacts, exhibiting low noise and large dynamic range (DR).[111]

Thanks to the vdWs interlayer connections without surface dangling bonds, the vertically stacked GaSe/MoS_2 heterostructure can be simply constructed by mechanical stacking (Inset of Figure 11c). The minimum obtained noise equivalent power (NEP) of GaSe/MoS_2 device is as low as around 10^{-14} $W/\sqrt{Hz}$ as shown in Figure 11c, revealing promising detection capability for illumination of sub-pW level theoretically. Furthermore, a large DR around 70 dB was calculated from the curves of photocurrent versus incident power (Figure 11d), which is even superior to that of the InGaAs based photodetectors (66 dB).[80] The ultralow NEP and large DR may result from the asymmetric metal-semiconductor contacts, which could suppress the dark current and optimize the photoresponse of the device.

Another recent example demonstrated a self-powered photodetector based on GaSe/WS_2 vertically p-n junction.[109] A pair of graphene films was employed as charge extraction electrodes, which could provide good quality of interface due to the vdWs connections with the 2D heterostructure (Inset of Figure 11e). Benefiting from the built-in electrical field of the heterostructure, the GaSe/WS_2 photodetector exhibits a large photoresponsivity of 56 mA/W and EQE of 16.97 % at zero bias, revealing typical characteristics of self-driven photodetectors. It is also worth noting that the photoresponsivity of the device reaches up to 149 A/W at bias of 2 V and fast response speed (rise time of ~37 μs), exhibiting superior photoresponse performance compared to the devices based on some other 2D heterojunctions.[114,115] Meanwhile, the GaSe/WS_2 photodetector presents the photoresponse spectrum from visible (740 nm) to UV (270 nm) region as shown in Figure 11e. Remarkably, the device under zero bias also shows relatively high photoresponsivity

from 270 to 680 nm, verifying that the ability of self-powered photodetection is also applicable in a broadband range.

Because of the large lattice mismatch between GaSe and TMDs, it is challenging to directly fabricate heterostructures between these materials in principle, which greatly hinders the structure to be integrated into practical applications. Recently, Li et al. have successfully fabricated both vertically stacked and lateral heterostructures based on GaSe and $MoSe_2$ monolayers by a novel two-step CVD method and demonstrated a gate-tunable photovoltaic device.[108] The vertical heterostructure shows clear epitaxial feature with misfit lattice matching. Conversely, in the lateral heterostructure, the GaSe monolayer has not shown any well alignment with the orientation of $MoSe_2$, but overgrown on $MoSe_2$ during the fabrication process, resulting in a stripe-like vertical heterostructure at the interface (Figure 11f). The rectifying current-voltage characteristics have been observed in this heterojunction, indicating the formation of p-n junction. Under the illumination of white light, clear photovoltaic response can be observed from the GaSe/$MoSe_2$ device (Figure 11g). At zero gate bias, the extracted open-circuit voltage (V_{oc}) and short-circuit current density (J_{sc}) are around 0.57 V and 0.35 mA/cm^2, respectively. Meanwhile, the main figure-of-merits (FOM) of solar cell, such as power conversion efficiency (PCE), fill factor have also been calculated to be 0.12 % and 0.38, respectively. All these values show a monotonic increasing trend with the gate biases. The results indicate that GaSe/$MoSe_2$ heterostructure has strong interlayer coupling and efficient separation of photocarriers, which is desirable for the development of 2D solar cells.

Besides 2D vdWs materials, ultrathin GaSe nanosheets have also been fabricated into heterostructures with some conventional semiconductors, such as silicon (Si), which

exhibits great potential for nano-electronic and optoelectronic applications thanks to both excellent semiconducting characteristics and 2D nature.[116] Recently, Yuan et al. have successfully fabricated vertically large-scale heterostructure based on p-type GaSe and n-type Si wafer by molecular beam epitaxy (MBE), and demonstrated an array of high-efficient photodetectors based on the structure.[116] In contrast to CVD method, MBE has superiority on synthesizing epitaxial wafer-scale heterostructures because the growth process can be *in situ* well controlled by the built-in reflection high-energy electron diffraction (RHEED).[117] For measuring optoelectronic properties, a patterned transparent indium-tin oxide (ITO) film was employed to enhance the light absorption of the heterostructure (Figure 11h). As shown in Figure 11i, a square corner of the GaSe/Si photodetector was illuminated by a 532 nm laser of 450 μW, exhibiting a clear and sharp-edged spatial-resolved photocurrent mapping image at zero bias. It should be noticed that the photocurrent is uniformly dispersed over the corner area of the ITO/GaSe/Si, which is consistent with the optical image of the junction. Quantitatively, the photodetector demonstrates excellent photoresponse performance with large EQE and short response time of 23.6 % and 60 μs, respectively. The response speed is much faster than the individual GaSe based photodetector.[21] Furthermore, the device shows remarkable stability by maintaining the performance after one million cycles of operation. The good performance of the GaSe/Si photodetector can be explained by the built-in potential induced from the depletion layer in GaSe and vertically electrical contacts.

4.1.2 GaTe heterostructures

As we introduced previously, 2D GaTe nanosheet is another member of III-VI group in favor of high sensitive photodetection applications thanks to its intrinsic direct band gap,

high carrier transport mobility and strong excitonic absorption at room temperature.[22,118,119] Meanwhile, the p-type semiconducting feature makes it desirable for fabricating 2D p-n junction with another n-type 2D semiconductor. Recently, a high performance self-driven photodetector has been developed based on ultrathin GaTe/MoS_2 p-n heterojunction, exhibiting fast and efficient photodetection ability.[37] Based on the results of DFT calculation, a type II heterojunction has been formed by the GaTe/MoS_2 heterostructure (**Figure 12**a). Under illumination of external light source, a mass of electron-hole pairs have been created, which can be separated efficiently exhibited by the built-in electric field in the p-n junction and the type II band alignment (Figure 12b). The photogenerated electrons and holes are then accumulated in GaTe and MoS_2 layers, respectively, resulting in considerable self-driven photocurrent within 10 ms. As shown in Figure 12c, a well-defined photoswitching characteristic can be observed, exhibiting a large photocurrent switching ratio up to 340, which is much larger than those of individual GaTe (switching ratio ~ 10) or MoS_2 (switching ratio ~ 85) devices. Meanwhile, the obtained photoresponsivity and EQE of the GaTe-MoS_2 device are 1.365 A/W and 266 %, respectively, which are superior to the photoresponse of MoS_2/Si device,[120] revealing good performance of self-driven photodetector.

Besides photodetection devices, 2D p-n junctions are also suitable for optoelectronic applications in photovoltaics by combing 2D semiconductors with desirable optical properties.[121,122] Recently, the combination of 2D p-type GaTe nanosheet and n-type InGaZnO (IGZO) thin film has been fabricated into transparent solar cell.[123] Both these two materials have direct band gap, which is propitious for the optoelectronic devices. Meanwhile, because of the large band gap and ultrathin thickness, the GaTe/IGZO

heterostructure is strongly transparent to the visible light with an average transmittance of 90.86 % by the transmittance measurement, which allows the fabrication of transparent solar cell device (Figure 12d). The photovoltaic performance of GaTe/IGZO device was characterized in vacuum circumstance under the illumination of a halogen lamp. With the intensity of incident light around 4.42 mW/cm^2, a large open-circuit voltage (V_{oc}) and short-circuit current density (J_{sc}) can be extracted to be 0.14 V and 0.63 mA/cm^2, respectively, verifying the GaTe/IGZO p-n junction working as a photovoltaic device. Remarkably, the PCE of the device was obtained as 0.73 % with a fill factor of 0.37 (Figure 12e), which shows superiority among the photovoltaic devices based on 2D-2D heterojunctions.[124,125] Furthermore, the time profile of photovoltaic response of GaTe/IGZO transparent solar cell has also been measured. As shown in Figure 12f, short-circuit current (I_{sc}) shows an instantaneously periodic response following the pulses of the incident light. Also, the I_{sc} induced by 400 nm light is larger than that of 500 nm light source, which may be attributed to the different absorption rate of GaTe/IGZO on the light wavelength. The mechanism of the device can be explained by the type II staggered-gap heterojunction formed at GaTe/IGZO, which could promote the separation of photogenerated electron-hole pairs.

4.2 InSe based heterostructures

Recently, 2D InSe nanosheets have been fabricated into vdWs heterostructures with a series of other 2D materials, including BP, graphene, GaSe et al., providing a new platform to develop multifunctional optoelectronic devices.[126–128] As a typical p-type 2D semiconductor, BP has been considered as a desirable candidate to form high performance 2D p-n junctions thanks to its tunable band gaps and outstanding electronic

properties.[129,130] As an example, Zhao et al. developed a vertical p-n diode based on p-BP and n-InSe, exhibiting highly polarized photodetection and fast photoresponse (**Figure 13**a).[36] The formation of vdWs p-n junction at the interface of BP and InSe was confirmed by the observation of clearly gate-tunable rectifying effect. As phosphorene possesses strong in-plane anisotropic property, it is intriguing to study the polarization photoresponse of the BP/InSe p-n junction. Thanks to the large light absorption coefficient and compact contact at the edge of the heterojunction, the photocurrent is spatially non-uniform distributed and mainly generated from the brink of the device. Meanwhile, the photocurrent is also sensitive to the polarization of the incident light. As shown in the inset of Figure 13a, clear modulation of photocurrent on the light polarization can be observed, revealing large anisotropy ratio of around 0.83, which is much superior to those of devices based on only 2D BP nanosheets.[131] Besides, the photodetector based on BP/InSe p-n junction exhibits broadband photodetection from visible (450 nm) to NIR (950 nm) region with remarkable photoresponsivity as large as 11.7 mA/W, which is similar to the performance of BP/MoS_2 junction.[129] It has also been found that the photoresponse of the device ascribes to both BP and InSe with equal contribution. The time profile of dynamic photoresponse has also been recorded during the on/off photo-switching process. The rise and fall response time of the BP/InSe photodetector are 24 ms and 32 ms, respectively as shown in Figure 13b. Such a fast response speed results from the high charge separation efficiency and large carrier transport mobility of BP/InSe heterostructure.[36]

Recently, 2D InSe has also been integrated with another III-VI semiconductor GaSe to form vdWs heterostructure, resulting in a fast and self-driven photodetector with broadband photoresponse.[126] As 2D GaSe nanosheets have larger band gap (2.05 eV) than

InSe (1.26 eV), it will allow the photons with energy (1.26 ~ 2.05 eV) to transmit and excite the electron-hole pairs in InSe layer. The device also employed graphene as the electrode to sandwich the p-GaSe/n-InSe heterostructure (inset of Figure 13c), which could provide a clean interface without dangling bonds and free of Fermi-level pinning. The photoresponse of the device can be observed at zero bias because of the built-in electrical field of GaSe/InSe and type II alignment, realizing photoresponsivity and detectivity of 21 mA/W and 2.2×10^{12} Jones at 410 nm, respectively. Moreover, a broadband spectral of photoresponse has been recorded in GaSe/InSe photodetector, covering from 270 nm (UV) to 920 nm (NIR), which is one of the largest photodetection region in 2D limit (Figure 13c).[9] In consistent with the previous study, the photoresponse in UV region here is induced by the interband absorption in the 2D GaSe nanosheets, while the NIR response can be explained by the interband transitions in the InSe nanosheets with smaller optical band gap.[21,23] Meanwhile, the device also exhibits extremely fast response speed with rise- and decay- time of 1.85 and 2.05 μs, respectively, which are substantially faster than those of other 2D vdWs heterostructures.[113,128] The fast and broadband photoresponse is attributed to the appealing optical properties of GaSe and InSe, and efficient generation and extraction of photocarriers induced by the graphene electrodes.

Apart from integration with 2D semiconductors, ultrathin InSe layer has also formed vdWs heterostructures with graphene, demonstrating proof-of-concept applications in electronic and optoelectronics.[132,133] Recently, Mudd et al. developed a broadband photodetector based on heterostructure of mechanical exfoliated InSe and CVD grown graphene nanosheets.[128] The device was constructed by transferring InSe nanosheets on top of the patterned graphene electrodes as shown in the inset of Figure 13d. The highest

obtained photoresponsivity is around 10^5 A/W at wavelength of 633 nm, which has not been achieved in other 2D heterojunctions upon the work published.[128] Meanwhile, a broadband photoresponse from visible to NIR can be observed under non-focused illumination as shown in Figure 13d. The photocurrent also shows weakly dependence on the gate biases. Such a sensitive photodetection can be explained by propitious band alignment at the interface of InSe and graphene.

Besides vertically constructed heterojunctions, the lateral p-n junctions based on 2D materials have also been developed in recent years, such as $MoSe_2$-WSe_2, which demonstrates applications in optoelectronics and allows to explore new functionalities of 2D devices.[134–136] More recently, Feng et al designed a high performance photodiode based on lateral heterostructure of InSe nanosheets and ultrathin copper indium diselenide ($CuInSe_2$) (inset of Figure 13e), which has been proved to be an efficient material for solar energy harvesting applications thanks to its high light absorption coefficient and direct band gap (~1.1 eV).[137] Thanks to the small band gaps of InSe and $CuInSe_2$, the InSe-$CuInSe_2$ device exhibits a broadband photoresponse from 254 nm (UV) to 850 nm (NIR), with photoresponsivity ranging from 0.5 A/W (850 nm) to 8.4 A/W (254 nm) (Figure 13e), which is around twenty folds larger than that of photodetector based on WSe_2 lateral heterostructure (210 mA/W at 532 nm).[136] Moreover, the photovoltaic performance of the device has been characterized because the p-n junction is also the fundamental component for the solar cells. The legible photovoltaic effect can be observed, where the open-circuit voltage and fill factor show linear relationship and independence of the light intensity, respectively as shown in Figure 13f. A large PCE was obtained around 3.5 % for 40 nm thick InSe-$CuInSe_2$ heterostructure, which is much greater to those of other 2D

heterostructures, such as WSe_2 lateral heterostructure, GaTe/IGZO p-n junction et al..[123,135] With increasing the channel thickness, the performance of the InSe-$CuInSe_2$ optoelectronic device would be enlarged thanks to the higher optical absorption. Overall, the direct band gap feature makes 2D InSe and its heterostructure promising for optoelectronic applications.

4.3 In_2Se_3 based heterostructures

Monolayer β-In_2Se_3 nanosheets have been fabricated into high performance photodetector with high photoresponsivity and fast response due to their large light absorption coefficient.[93] Recently, a broadband photodetector array was developed based on large-scale β-In_2Se_3/Si p-n heterojunction, which was prepared by PLD method.[138] The combination of 2D semiconductor with silicon technology paves the way to construct high performance practical devices by exploiting the advantages of both material systems. The β-In_2Se_3/Si p-n junction exhibits a type II staggered band alignment according to the band diagram (**Figure 14**a), which benefits for the separation of photogenerated electron-hole pairs and further increases the photocurrent at the same drain bias. The FOM of the device at 532 nm light illumination were obtained as photoresponsivity of 5.9 A/W, EQE of 1376 % and detectivity of 4.9×10^{12} Jones, which is superior or comparable to those of photodetectors based on individual In_2Se_3 nanosheets.[89,93,95] The array consisted of 84 photodetectors in the heterojunction also presents highly uniform performance, revealing homogeneous growth of the large-area 2D heterostructure. Moreover, β-In_2Se_3/Si photodetectors show the broadband photodetection ability across from UV (370 nm) to NIR (808 nm) (Figure 14b), exhibiting extremely high detectivity at all illumination wavelength, which is favorable for the detection of weak signal. As shown in Figure 14c,

the device even shows distinct response to the lighter in ambient, indicating desirable ability for weak signal detection.

Benefiting from the advantages of both 2D In_2Se_3 and $CuInSe_2$ thin film, a high performance photodetector was developed based on the lateral p-n heterojunction fabricated by these two materials.[106] The band structure of In_2Se_3-$CuInSe_2$ was measured by ultraviolet photoelectron spectroscopy (UPS), exhibiting a typical type-II band alignment (Figure 14d). Same as InSe-$CuInSe_2$ heterojunction, the type-II junction could enhance the photodetection by optimizing the separation efficiency of photoexcited electron-hole pairs due to the synergistic effects. As a result, the In_2Se_3-$CuInSe_2$ photodetector exhibits a high photoresponsivity of 20.1 A/W, which is around 7.5 times larger than that of device based on sole In_2Se_3 under idential measurement conditions. As shown in Figure 14e, the EQEs are largely dependent on the illumination intensity and the maximum magnitudes of EQEs for In_2Se_3-$CuInSe_2$ and In_2Se_3 photodetectors are 4698 and 629 %, respectively, revealing remarkable enhancement of photoresponse due to the formation of p-n junction.[133] Moreover, a broadband photodetection was obtained in In_2Se_3-$CuInSe_2$ photodetector (Figure 14f). The photoresponse spectral range covers from 370 nm to 1550 nm, which is much broader than that of InSe-$CuInSe_2$ lateral heterojunction.[137] As it is rare to cover 1550 nm for 2D photodetectors, In_2Se_3-$CuInSe_2$ p-n heterojunction demonstrates a feasible approach for photodetection in NIR region.

5. Conclusions and outlook

The great interests on 2D materials have motivated a revisit on the layered group III-VI semiconductors, which possesses many unique electrical and optical properties which are

not found in either TMD family or phosphorene. The direct, thickness dependent band gaps and large carrier transport mobility make them a potential candidate for developing optoelectronic applications at nanoscale. In this review, the recent advances of optoelectronic devices based on 2D III-VI semiconductors and their heterostructures have been systematically summarized. The crystal structure and optical properties of group III-VI have been briefly introduced at first, indicating wide range of tunable band gaps and unique band gap from direct to indirect transition along with decreasing of layer number. The overview of optoelectronic applications has been categorized by different stoichiometric composition, which illustrates in the sequence of gallium monochalcogenides, indium monochalcogenides, In_2X_3 (X=S, Se, Te) and their heterostructures. Based on the previously studies, 2D III-VI semiconductors are mainly exploited in the applications of photodetection and light-harvesting devices. The design, characterization and optimization of 2D III-VI based photodetectors or solar cells on either rigid or flexible substrates are described. **Table 2** summarizes the main FOM of photo-sensing devices based on ultrathin III-VI nanosheets and several other typical 2D layered materials. It is worth noting that most of III-VI semiconductors based photodetectors exhibit broader spectral range and larger detectivity than those of TMDs or BP. Meanwhile, the comparison of performance of photovoltaic devices based on group III-VI semiconductors and other 2D materials is shown in **Table 3**. The FF and PCE of 2D III-VI solar cells are comparable to those of graphene, MoS_2 or phosphorene based heterostructures. In a word, 2D III-VI semiconductors are desirable for developing high performance optoelectronic applications in 2D limit.

So far, the device demonstration of III-VI semiconductors have just entered in the incipient stage. In the next few years, new techniques to realize large-scale, good crystallinity and controllable growth of ultrathin III-VI materials are still highly desirable. The performance of present devices will be optimized and some new type of optoelectronic applications will be developed. Meanwhile, wearable and transparent devices will also be explored. Compared to those materials conventionally used in optoelectronic applications (e.g., III-V and II-VI semiconductors), 2D III-VI semiconductors exhibit tunable band gap in a broad range. To compete with conventional semiconductors, some challenges and opportunities need to be addressed.

1. Besides photodetection and photovoltaic devices, LEDs are also one of the significant types of optoelectronic applications, which is important for lighting, display and optical communication applications.[140] Previously, 2D inorganic LEDs are mainly designed based on semiconducting layered TMDs, exhibiting high efficiency and low turn-on current.[141,142] However, to the best of our knowledge, the electroluminescent devices based on layered III-VI family have not been reported yet. The direct band gaps of few-layer III-VI semiconductors have fulfilled the basic requirement of light emission. Previous work has shown that electroluminescence (EL) can be observed from the homojunction p-InSe/n-InSe and heterojunction p-GaSe/n-InSe, respectively at room temperature.[143] However, either of these two structures has not yet been demonstrated as a device. The luminescence efficiency and linewidth are unknown. Moreover, achieving high quantum yield of PL and high quality samples are additional challenges to realize 2D LEDs.

2. The scalable growth of high quality 2D III-VI thin films without domain boundary and dislocations are significant for fabricating practical optoelectronic devices, which is also

one of the main problems demanding prompt solutions for the whole 2D family. Although CVD has been proved as an effective technique to prepare large-area samples, it seems not suitable for preparation of some chemically unstable materials, such as InSe. Our recent work has successfully synthesized wafer-scale layered InSe thin films by PLD, and demonstrated phototransistors with broadband photoresponse.[44] However, the polycrystalline structure and defects induced by the energetic laser pulses are still required to be optimized for achieving higher device performance. In addition, the direct growth of large area III-VI based 2D heterostructures has not been achieved as well. Therefore, the new synthesis techniques are still desired to realize scalable, continuous, homogeneous growth and good controlling on layer number. Moreover, the package and chemical passivation methods are also required to be developed to solve the instability problem of ultrathin III-VI samples, which could also further improve the performance of related optoelectronic devices.

3. Recently, the piezo-phototronic effect, which applies piezoelectric potential to control the generation, transport, separation and/or recombination of carriers, has been employed to improve the performance of optoelectronic devices.[52,144–147] So far, several 2D piezoelectric materials have been presented, such as MoS_2, BN.[148] It has been reported that monolayer group III-VI semiconductors are also piezoelectric from the theoretical view, exhibiting similar piezoelectric coefficients as those of BN and MoS_2.[55,57] As we mentioned before, so far, the observation of piezoelectric and piezo-phototronic effects in III-VI semiconductors is only from layered GaSe nanosheets.[59] However, the study is still in the starting stage and the thickness of GaSe nanosheets is relatively thick. Further investigation to realize tunable photodetection and great enhancement of photoresponsivity

are required. Furthermore, the development of piezo-phototronic devices should be extended to more 2D III-VI materials and their heterostructures.

Thanks to the widely tunable band gaps and luxuriant characteristics induced by the diverse polytypes, 2D layered III-VI semiconductors have expressed great potential in optoelectronic applications, as evidenced by a number of the previously reported proof-of-concept photo-sensing and photovoltaic devices. It is foreseen that further advances in wafer-scale fabrication and device characterization of III-VI materials and heterostructures would lead to practical optoelectronic devices in the future.

Acknowledgements

This work is supported by the Research Grants Council (RGC) of Hong Kong (RGC GRF No. PolyU 153023/18P).

Conflict of Interest

The authors declare no conflict of interest.

References

[1] Q. H. Wang, K. Kalantar-Zadeh, A. Kis, J. N. Coleman, M. S. Strano, *Nat. Nanotechnol.* **2012**, *7*, 699.

[2] K. S. Novoselov, A. Mishchenko, A. Carvalho, A. H. Castro Neto, *Science* **2016**, *353*, aac9439.

[3] B. Radisavljevic, A. Kis, *Nat. Mater.* **2013**, *12*, 815.

[4] S. Z. Butler, S. M. Hollen, L. Cao, Y. Cui, J. A. Gupta, H. R. Gutiérrez, T. F. Heinz, S. S. Hong, J. Huang, A. F. Ismach, E. Johnston-Halperin, M. Kuno, V. V. Plashnitsa, R. D. Robinson, R. S. Ruoff, S. Salahuddin, J. Shan, L. Shi, M. G. Spencer, M. Terrones, W. Windl, J. E. Goldberger, *ACS Nano* **2013**, *7*, 2898.

[5] J. N. Coleman, U. Khan, K. Young, A. Gaucher, S. De, R. J. Smith, I. V Shvets, S. K. Arora, G. Stanton, H. Kim, K. Lee, G. T. Kim, G. S. Duesberg, T. Hallam, J. J. Boland, J. J. Wang, J. F. Donegan, J. C. Grunlan, G. Moriarty, A. Shmeliov, R. J. Nicholls, J. M. Perkins, E. M. Grieveson, K. Theuwissen, D. W. Mccomb, P. D. Nellist, V. Nicolosi, *Science* **2013**, *331*, 568.

[6] A. J. Mannix, B. Kiraly, M. C. Hersam, N. P. Guisinger, *Nat. Rev. Chem.* **2017**, *1*, 0014.

[7] S. Yuan, Z. Yang, C. Xie, F. Yan, J. Dai, S. P. Lau, H. L. W. Chan, J. Hao, *Adv. Mater.* **2016**, *28*, 10048.

[8] D. Jariwala, V. K. Sangwan, L. J. Lauhon, T. J. Marks, M. C. Hersam, *ACS Nano* **2014**, *8*, 1102.

[9] L. Li, Y. Yu, G. J. Ye, Q. Ge, X. Ou, H. Wu, D. Feng, X. H. Chen, Y. Zhang, *Nat. Nanotechnol.* **2014**, *9*, 372.

[10] L. Tao, E. Cinquanta, D. Chiappe, C. Grazianetti, M. Fanciulli, M. Dubey, A. Molle, D. Akinwande, *Nat. Nanotechnol.* **2015**, *10*, 227.

[11] G. Bai, S. Yuan, Y. Zhao, Z. Yang, S. Y. Choi, Y. Chai, S. F. Yu, S. P. Lau, J. Hao, *Adv. Mater.* **2016**, *28*, 7472.

[12] H. Li, X. Wang, X. Zhu, X. Duan, A. Pan, *Chem. Soc. Rev.* **2018**, *47*, 7504.

[13] X. Song, J. Hu, H. Zeng, *J. Mater. Chem. C* **2013**, *1*, 2952.

[14] A. Allain, J. Kang, K. Banerjee, A. Kis, *Nat. Mater.* **2015**, *14*, 1195.

[15] J. Shim, H.-Y. Park, D.-H. Kang, J.-O. Kim, S.-H. Jo, Y. Park, J.-H. Park, *Adv. Electron. Mater.* **2017**, *3*, 1600364.

[16] G. Bai, Z. Yang, H. Lin, W. Jie, J. Hao, *Nanoscale* **2018**, *10*, 9261.

[17] O. Lopez-Sanchez, D. Lembke, M. Kayci, A. Radenovic, A. Kis, *Nat. Nanotechnol.* **2013**, *8*, 497.

[18] R. Cheng, D. Li, H. Zhou, C. Wang, A. Yin, S. Jiang, Y. Liu, Y. Chen, Y. Huang, X. Duan, *Nano Lett.* **2014**, *14*, 5590.

[19] W. Huang, L. Gan, H. Li, Y. Ma, T. Zhai, *CrystEngComm* **2016**, *18*, 3968.

[20] K. Xu, L. Yin, Y. Huang, T. A. Shifa, J. Chu, F. Wang, R. Cheng, Z. Wang, J. He, *Nanoscale* **2016**, *8*, 16802.

[21] P. Hu, Z. Wen, L. Wang, P. Tan, K. Xiao, *ACS Nano* **2012**, *6*, 5988.

[22] F. Liu, H. Shimotani, H. Shang, T. Kanagasekaran, V. Zólyomi, N. Drummond, V. I. Fal'Ko, K. Tanigaki, *ACS Nano* **2014**, *8*, 752.

[23] G. W. Mudd, S. A. Svatek, T. Ren, A. Patanè, O. Makarovsky, L. Eaves, P. H. Beton, Z. D. Kovalyuk, G. V Lashkarev, Z. R. Kudrynskyi, *Adv. Mater.* **2013**, *25*, 5714.

[24] J. O. Island, S. I. Blanter, M. Buscema, H. S. J. Van Der Zant, A. Castellanos-Gomez, *Nano Lett.* **2015**, *15*, 7853.

[25] W. Huang, L. Gan, H. Yang, N. Zhou, R. Wang, W. Wu, H. Li, Y. Ma, H. Zeng, T. Zhai, *Adv. Funct. Mater.* **2017**, *27*, 1702448.

[26] G. Han, Z.-G. Chen, C. Sun, L. Yang, L. Cheng, Z. Li, W. Lu, Z. M. Gibbs, G. J. Snyder, K. Jack, J. Drennan, J. Zou, *CrystEngComm* **2014**, *16*, 393.

[27] S. Lei, L. Ge, S. Najmaei, A. George, R. Kappera, J. Lou, M. Chhowalla, H. Yamaguchi, G. Gupta, R. Vajtai, A. D. Mohite, P. M. Ajayan, *ACS Nano* **2014**, *8*, 1263.

[28] P. Hu, L. Wang, M. Yoon, J. Zhang, W. Feng, X. Wang, Z. Wen, J. C. Idrobo, Y. Miyamoto, D. B. Geohegan, K. Xiao, *Nano Lett.* **2013**, *13*, 1649.

[29] M. Brotons-Gisbert, D. Andres-Penares, J. Suh, F. Hidalgo, R. Abargues, P. J. Rodríguez-Cantó, A. Segura, A. Cros, G. Tobias, E. Canadell, *Nano Lett.* **2016**, *16*, 3221.

[30] W. Feng, W. Zheng, W. Cao, P. Hu, *Adv. Mater.* **2014**, *26*, 6587.

[31] S. R. Tamalampudi, Y.-Y. Lu, R. Kumar U, R. Sankar, C.-D. Liao, K. Moorthy B, C.-H. Cheng, F. C. Chou, Y.-T. Chen, *Nano Lett.* **2014**, *14*, 2800.

[32] L. Jiao, W. Jie, Z. Yang, Y. Wang, Z. Chen, X. Zhang, W. Tang, Z. Wu, J. Hao, *J. Mater. Chem. C* **2019**, *7*, 2522.

[33] Y. Xue, Y. Zhang, Y. Liu, H. Liu, J. Song, J. Sophia, J. Liu, Z. Xu, Q. Xu, Z. Wang, J. Zheng, Y. Liu, S. Li, Q. Bao, *ACS Nano* **2016**, *10*, 573.

[34] A. K. Geim, I. V Grigorieva, *Nature* **2013**, *499*, 419.

[35] Y. Liu, N. O. Weiss, X. Duan, H.-C. Cheng, Y. Huang, X. Duan, *Nat. Rev. Mater.* **2016**, *1*, 16042.

[36] S. Zhao, J. Wu, K. Jin, H. Ding, T. Li, C. Wu, N. Pan, X. Wang, *Adv. Funct. Mater.* **2018**, *28*, 1802011.

[37] S. Yang, C. Wang, C. Ataca, Y. Li, H. Chen, H. Cai, A. Suslu, J. C. Grossman, C. Jiang, Q. Liu, S. Tongay, *ACS Appl. Mater. Interfaces* **2016**, *8*, 2533.

[38] X. Zhou, J. Cheng, Y. Zhou, T. Cao, H. Hong, Z. Liao, S. Wu, H. Peng, K. Liu, D.

Yu, *J. Am. Chem. Soc.* **2015**, *137*, 7994.

[39] X. Li, M. W. Lin, A. A. Puretzky, J. C. Idrobo, C. Ma, M. Chi, M. Yoon, C. M. Rouleau, I. I. Kravchenko, D. B. Geohegan, K. Xiao, *Sci. Rep.* **2014**, *4*, 5497.

[40] W. Jie, X. Chen, D. Li, L. Xie, Y. Y. Hui, S. P. Lau, X. Cui, J. Hao, *Angew. Chemie Int. Ed.* **2015**, *54*, 1185.

[41] K. F. Mak, C. Lee, J. Hone, J. Shan, T. F. Heinz, *Phys. Rev. Lett.* **2010**, *105*, 136805.

[42] D. A. Bandurin, A. V. Tyurnina, G. L. Yu, A. Mishchenko, V. Zólyomi, S. V. Morozov, R. K. Kumar, R. V. Gorbachev, Z. R. Kudrynskyi, S. Pezzini, Z. D. Kovalyuk, U. Zeitler, K. S. Novoselov, A. Patanè, L. Eaves, I. V. Grigorieva, V. I. Fal'ko, A. K. Geim, Y. Cao, *Nat. Nanotechnol.* **2016**, *12*, 223.

[43] A. A. Kistanov, Y. Cai, K. Zhou, S. V. Dmitriev, Y. W. Zhang, *J. Mater. Chem. C* **2018**, *6*, 518.

[44] Z. Yang, W. Jie, C.-H. Mak, S. Lin, H. Lin, X. Yang, F. Yan, S. P. Lau, J. Hao, *ACS Nano* **2017**, *11*, 4225.

[45] S. Lei, L. Ge, Z. Liu, S. Najmaei, G. Shi, G. You, J. Lou, R. Vajtai, P. M. Ajayan, *Nano Lett.* **2013**, *13*, 2777.

[46] Y. Yang, H. Du, Q. Xue, X. Wei, Z. Yang, C. Xu, D. Lin, W. Jie, J. Hao, *Nano Energy* **2019**, *57*, 566.

[47] M. Mahjouri-Samani, R. Gresback, M. Tian, K. Wang, A. A. Puretzky, C. M. Rouleau, G. Eres, I. N. Ivanov, K. Xiao, M. A. McGuire, G. Duscher, D. B. Geohegan, *Adv. Funct. Mater.* **2014**, *24*, 6365.

[48] Y. Zhou, Y. Zhou, Y. Nie, Y. Liu, K. Yan, J. Hong, C. Jin, J. Yin, Z. Liu, H. Peng,

ACS Nano **2014**, *8*, 1485.

[49] S. Yang, Q. Yue, H. Cai, K. Wu, C. Jiang, S. Tongay, *J. Mater. Chem. C* **2016**, *4*, 248.

[50] H. Li, Z. Yin, Q. He, H. Li, X. Huang, G. Lu, D. W. H. Fam, A. I. Y. Tok, Q. Zhang, H. Zhang, *Small* **2012**, *8*, 63.

[51] D. J. Late, Y.-K. Huang, B. Liu, J. Acharya, S. N. Shirodkar, J. Luo, A. Yan, D. Charles, U. V. Waghmare, V. P. Dravid, C. N. R. Rao, *ACS Nano* **2013**, *7*, 4879.

[52] Z. L. Wang, *Adv. Mater.* **2012**, *24*, 4632.

[53] W. Wu, Z. L. Wang, *Nat. Rev. Mater.* **2016**, *1*, 16031.

[54] Y. Zhang, G. Gao, H. L. W. Chan, J. Dai, Y. Wang, J. Hao, *Adv. Mater.* **2012**, *24*, 1729.

[55] W. Wu, L. Wang, Y. Li, F. Zhang, L. Lin, S. Niu, D. Chenet, X. Zhang, Y. Hao, T. F. Heinz, J. Hone, Z. L. Wang, *Nature* **2014**, *514*, 470.

[56] W. Wu, L. Wang, R. Yu, Y. Liu, S.-H. Wei, J. Hone, Z. L. Wang, *Adv. Mater.* **2016**, *28*, 8463.

[57] W. Li, J. Li, *Nano Res.* **2015**, *8*, 3796.

[58] Y. Wu, H.-R. Fuh, D. Zhang, C. Ó. Coileáin, H. Xu, J. Cho, M. Choi, B. S. Chun, X. Jiang, M. Abid, M. Abid, H. Liu, J. J. Wang, I. V. Shvets, C.-R. Chang, H.-C. Wu, *Nano Energy* **2017**, *32*, 157.

[59] T. Jia, H. R. Fuh, D. Chen, M. Abid, M. Abid, D. Zhang, A. B. Sarker, J. Cho, M. Choi, B. S. Chun, H. Xu, C. Ó Coileáin, H. Liu, C. R. Chang, H. C. Wu, *Adv. Electron. Mater.* **2018**, *4*, 1700447.

[60] S. Yang, Y. Li, X. Wang, N. Huo, J.-B. Xia, S.-S. Li, J. Li, *Nanoscale* **2014**, *6*,

2582.

[61] S. Huang, Y. Tatsumi, X. Ling, H. Guo, Z. Wang, G. Watson, A. A. Puretzky, D. B. Geohegan, J. Kong, J. Li, T. Yang, R. Saito, M. S. Dresselhaus, *ACS Nano* **2016**, *10*, 8964.

[62] Z. Wang, M. Safdar, M. Mirza, K. Xu, Q. Wang, Y. Huang, F. Wang, X. Zhan, J. He, *Nanoscale* **2015**, *7*, 7252.

[63] Z. Wang, K. Xu, Y. Li, X. Zhan, M. Safdar, Q. Wang, F. Wang, J. He, *ACS Nano* **2014**, *8*, 4859.

[64] T. Zheng, Z. T. Wu, H. Y. Nan, Y. F. Yu, A. Zafar, Z. Z. Yan, J. P. Lu, Z. H. Ni, *RSC Adv.* **2017**, *7*, 54964.

[65] J. Lauth, F. E. S. Gorris, M. Samadi Khoshkhoo, T. Chassé, W. Friedrich, V. Lebedeva, A. Meyer, C. Klinke, A. Kornowski, M. Scheele, H. Weller, *Chem. Mater.* **2016**, *28*, 1728.

[66] H.-C. Chang, C.-L. Tu, K.-I. Lin, J. Pu, T. Takenobu, C.-N. Hsiao, C.-H. Chen, *Small* **2018**, 1802351.

[67] Z. Yin, H. Li, H. Li, L. Jiang, Y. Shi, Y. Sun, G. Lu, Q. Zhang, X. Chen, H. Zhang, *ACS Nano* **2012**, *6*, 74.

[68] W. Choi, M. Y. Cho, A. Konar, J. H. Lee, G.-B. Cha, S. C. Hong, S. Kim, J. Kim, D. Jena, J. Joo, S. Kim, *Adv. Mater.* **2012**, *24*, 5832.

[69] Y.-H. Lee, X.-Q. Zhang, W. Zhang, M.-T. Chang, C.-T. Lin, K.-D. Chang, Y.-C. Yu, J. T.-W. Wang, C.-S. Chang, L.-J. Li, T.-W. Lin, *Adv. Mater.* **2012**, *24*, 2320.

[70] K. S. Kim, Y. Zhao, H. Jang, S. Y. Lee, J. M. Kim, K. S. Kim, J.-H. Ahn, P. Kim, J.-Y. Choi, B. H. Hong, *Nature* **2009**, *457*, 706.

[71] Z. Yang, J. Hao, S. Yuan, S. Lin, H. M. Yau, J. Dai, S. P. Lau, *Adv. Mater.* **2015**, *27*, 3748.

[72] Z. Yang, J. Hao, *J. Mater. Chem. C* **2016**, *4*, 8859.

[73] W. Jie, Z. Yang, F. Zhang, G. Bai, C. W. Leung, J. Hao, *ACS Nano* **2017**, *11*, 6950.

[74] Z. Li, H. Qiao, Z. Guo, X. Ren, Z. Huang, X. Qi, S. C. Dhanabalan, J. S. Ponraj, D. Zhang, J. Li, J. Zhao, J. Zhong, H. Zhang, *Adv. Funct. Mater.* **2018**, *28*, 1705237.

[75] S. H. Yu, Y. Lee, S. K. Jang, J. Kang, J. Jeon, C. Lee, J. Y. Lee, H. Kim, E. Hwang, S. Lee, J. H. Cho, *ACS Nano* **2014**, *8*, 8285.

[76] J. Miao, W. Hu, Y. Jing, W. Luo, L. Liao, A. Pan, S. Wu, J. Cheng, X. Chen, W. Lu, *Small* **2015**, *11*, 2392.

[77] X. Wang, P. Wang, J. Wang, W. Hu, X. Zhou, N. Guo, H. Huang, S. Sun, H. Shen, T. Lin, M. Tang, L. Liao, A. Jiang, J. Sun, X. Meng, X. Chen, W. Lu, J. Chu, *Adv. Mater.* **2015**, *27*, 6575.

[78] X. Li, J. Zhu, B. Wei, *Chem. Soc. Rev.* **2016**, *45*, 3145.

[79] Y. Li, Z. Li, C. Chi, H. Shan, L. Zheng, Z. Fang, *Adv. Sci.* **2017**, *4*, 1600430.

[80] M. Dai, H. Chen, R. Feng, W. Feng, Y. Hu, H. Yang, G. Liu, X. Chen, J. Zhang, C.-Y. Xu, P. Hu, *ACS Nano* **2018**, *12*, 8739.

[81] Y. R. Chang, P. H. Ho, C. Y. Wen, T. P. Chen, S. S. Li, J. Y. Wang, M. K. Li, C. A. Tsai, R. Sankar, W. H. Wang, P. W. Chiu, F. C. Chou, C. W. Chen, *ACS Photonics* **2017**, *4*, 2930.

[82] C. H. Ho, Y. J. Chu, *Adv. Opt. Mater.* **2015**, *3*, 1750.

[83] S. Lei, F. Wen, L. Ge, S. Najmaei, A. George, Y. Gong, W. Gao, Z. Jin, B. Li, J. Lou, J. Kono, R. Vajtai, P. Ajayan, N. J. Halas, *Nano Lett.* **2015**, *15*, 3048.

[84] W. Feng, J. Bin Wu, X. Li, W. Zheng, X. Zhou, K. Xiao, W. Cao, B. Yang, J. C. Idrobo, L. Basile, W. Tian, P. H. Tan, P. A. Hu, *J. Mater. Chem. C* **2015**, *3*, 7022.

[85] C. H. Ho, Y. H. Chen, J. H. Ho, *RSC Adv.* **2016**, *6*, 97445.

[86] M. A. . Seyam, *Vacuum* **2001**, *63*, 441.

[87] C.-H. Ho, *2D Mater.* **2016**, *3*, 025019.

[88] J. Quereda, R. Biele, G. Rubio-Bollinger, N. Agraït, R. D'Agosta, A. Castellanos-Gomez, *Adv. Opt. Mater.* **2016**, *4*, 1939.

[89] J. Zhou, Q. Zeng, D. Lv, L. Sun, L. Niu, W. Fu, F. Liu, Z. Shen, C. Jin, Z. Liu, *Nano Lett.* **2015**, *15*, 6400.

[90] W. Ding, J. Zhu, Z. Wang, Y. Gao, D. Xiao, Y. Gu, Z. Zhang, W. Zhu, *Nat. Commun.* **2017**, *8*, 14956.

[91] N. Balakrishnan, C. R. Staddon, E. F. Smith, J. Stec, D. Gay, G. W. Mudd, O. Makarovsky, Z. R. Kudrynskyi, Z. D. Kovalyuk, L. Eaves, A. Patanè, P. H. Beton, *2D Mater.* **2016**, *3*, 025030.

[92] N. Balakrishnan, E. D. Syteer, E. F. Smith, Z. R. Kudrynskyi, Z. D. Kovalyuk, L. Evaes, A. Patanè, P. H. Beton, *2D Mater.* **2018**, *5*, 035026.

[93] M. Lin, D. Wu, Y. Zhou, W. Huang, W. Jiang, W. Zheng, S. Zhao, C. Jin, Y. Guo, H. Peng, Z. Liu, *J. Am. Chem. Soc.* **2013**, *135*, 13274.

[94] Z. Q. Zheng, J. D. Yao, G. W. Yang, *J. Mater. Chem. C* **2016**, *4*, 8094.

[95] R. B. Jacobs-Gedrim, M. Shanmugam, N. Jain, C. A. Durcan, M. T. Murphy, T. M. Murray, R. J. Matyi, R. L. Moore, B. Yu, *ACS Nano* **2014**, *8*, 514.

[96] G. Almeida, S. Dogan, G. Bertoni, C. Giannini, R. Gaspari, S. Perissinotto, R. Krahne, S. Ghosh, L. Manna, *J. Am. Chem. Soc.* **2017**, *139*, 3005.

[97] C. Julien, A. Chevy, D. Siapkas, *Phys. status solidi* **1990**, *118*, 553.

[98] M. M. Furchi, D. K. Polyushkin, A. Pospischil, T. Mueller, *Nano Lett.* **2014**, *14*, 6165.

[99] M. Buscema, J. O. Island, D. J. Groenendijk, S. I. Blanter, G. A. Steele, H. S. J. van der Zant, A. Castellanos-Gomez, *Chem. Soc. Rev.* **2015**, *44*, 3691.

[100] R. Diehl, R. Nitsche, *J. Cryst. Growth* **1975**, *28*, 306.

[101] Y. H. Kim, J. H. Lee, D.-W. Shin, S. M. Park, J. S. Moon, J. G. Nam, J.-B. Yoo, *Chem. Commun.* **2010**, *46*, 2292.

[102] Z. Yang, J. Hao, *Small Methods* **2018**, *2*, 1700296.

[103] W. Jie, Z. Yang, G. Bai, J. Hao, *Adv. Opt. Mater.* **2018**, *6*, 1701296.

[104] M. Z. Bellus, Z. Yang, P. Zereshki, J. Hao, S. P. Lau, H. Zhao, *Nanoscale Horizons* **2019**, *4*, 236.

[105] N. Zhou, R. Wang, X. Zhou, H. Song, X. Xiong, Y. Ding, J. Lü, L. Gan, T. Zhai, *Small* **2018**, *14*, 1702731.

[106] X. Wei, F. Yan, Q. Lv, C. Shen, K. Wang, *Nanoscale* **2017**, *9*, 8388.

[107] R. Lu, J. Liu, H. Luo, V. Chikan, J. Z. Wu, *Sci. Rep.* **2016**, *6*, 19161.

[108] X. Li, M.-W. Lin, J. Lin, B. Huang, A. A. Puretzky, C. Ma, K. Wang, W. Zhou, S. T. Pantelides, M. Chi, I. Kravchenko, J. Fowlkes, C. M. Rouleau, D. B. Geohegan, K. Xiao, *Sci. Adv.* **2016**, *2*, e1501882.

[109] Q. Lv, F. Yan, X. Wei, K. Wang, *Adv. Opt. Mater.* **2017**, *6*, 1700490.

[110] W. Kim, C. Li, F. A. Chaves, D. Jiménez, R. D. Rodriguez, J. Susoma, M. A.

Fenner, H. Lipsanen, J. Riikonen, *Adv. Mater.* **2016**, *28*, 1845.

[111] A. Islam, J. Lee, P. X.-L. Feng, *ACS Photonics* **2018**, *5*, 2693.

[112] F. Xia, H. Wang, D. Xiao, M. Dubey, A. Ramasubramaniam, *Nat. Photonics* **2014**, *8*, 899.

[113] K. Roy, M. Padmanabhan, S. Goswami, T. P. Sai, G. Ramalingam, S. Raghavan, A. Ghosh, *Nat. Nanotechnol.* **2013**, *8*, 826.

[114] J. Yao, Z. Zheng, G. Yang, *J. Mater. Chem. C* **2016**, *4*, 7831.

[115] L. Ye, H. Li, Z. Chen, J. Xu, *ACS Photonics* **2016**, *3*, 692.

[116] X. Yuan, L. Tang, S. Liu, P. Wang, Z. Chen, C. Zhang, Y. Liu, W. Wang, Y. Zou, C. Liu, N. Guo, J. Zou, P. Zhou, W. Hu, F. Xiu, *Nano Lett.* **2015**, *15*, 3571.

[117] H. C. Diaz, R. Chaghi, Y. Ma, M. Batzill, *2D Mater.* **2015**, *2*, 044010.

[118] D. N. Bose, S. Pal, *Phys. Rev. B* **2001**, *63*, 235321.

[119] P. Hu, J. Zhang, M. Yoon, X. F. Qiao, X. Zhang, W. Feng, P. Tan, W. Zheng, J. Liu, X. Wang, J. C. Idrobo, D. B. Geohegan, K. Xiao, *Nano Res.* **2014**, *7*, 694.

[120] O. Lopez-Sanchez, E. Alarcon Llado, V. Koman, A. Fontcuberta i Morral, A. Radenovic, A. Kis, *ACS Nano* **2014**, *8*, 3042.

[121] S. Lin, X. Li, P. Wang, Z. Xu, S. Zhang, H. Zhong, Z. Wu, W. Xu, H. Chen, *Sci. Rep.* **2015**, *5*, 15103.

[122] M.-L. Tsai, S.-H. Su, J.-K. Chang, D.-S. Tsai, C.-H. Chen, C.-I. Wu, L.-J. Li, L.-J. Chen, J.-H. He, *ACS Nano* **2014**, *8*, 8317.

[123] A. J. Cho, K. Park, S. Park, M. K. Song, K. B. Chung, J. Y. Kwon, *J. Mater. Chem. C* **2017**, *5*, 4327.

[124] X. Wang, L. Huang, Y. Peng, N. Huo, K. Wu, C. Xia, Z. Wei, S. Tongay, J. Li,

Nano Res. **2016**, *9*, 507.

[125] M. M. Furchi, A. Pospischil, F. Libisch, J. Burgdörfer, T. Mueller, *Nano Lett.* **2014**, *14*, 4785.

[126] F. Yan, L. Zhao, A. Patanè, P. Hu, X. Wei, W. Luo, D. Zhang, Q. Lv, Q. Feng, C. Shen, K. Chang, L. Eaves, K. Wang, *Nanotechnology* **2017**, *28*, 27LT01.

[127] Y. M. Ding, J. J. Shi, C. Xia, M. Zhang, J. Du, P. Huang, M. Wu, H. Wang, Y. L. Cen, S. H. Pan, *Nanoscale* **2017**, *9*, 14682.

[128] G. W. Mudd, S. A. Svatek, L. Hague, O. Makarovsky, Z. R. Kudrynskyi, C. J. Mellor, P. H. Beton, L. Eaves, K. S. Novoselov, Z. D. Kovalyuk, E. E. Vdovin, A. J. Marsden, N. R. Wilson, A. Patanè, *Adv. Mater.* **2015**, *27*, 3760.

[129] Y. Deng, Z. Luo, N. J. Conrad, H. Liu, Y. Gong, S. Najmaei, P. M. Ajayan, J. Lou, X. Xu, P. D. Ye, *ACS Nano* **2014**, *8*, 8292.

[130] P. Gehring, R. Urcuyo, D. L. Duong, M. Burghard, K. Kern, *Appl. Phys. Lett.* **2015**, *106*, 233110.

[131] T. Hong, B. Chamlagain, W. Lin, H.-J. Chuang, M. Pan, Z. Zhou, Y.-Q. Xu, *Nanoscale* **2014**, *6*, 8978.

[132] Z. Chen, J. Biscaras, A. Shukla, *Nanoscale* **2015**, *7*, 5981.

[133] Z. R. Kudrynskyi, M. A. Bhuiyan, O. Makarovsky, J. D. G. Greener, E. E. Vdovin, Z. D. Kovalyuk, Y. Cao, A. Mishchenko, K. S. Novoselov, P. H. Beton, L. Eaves, A. Patanè, *Phys. Rev. Lett.* **2017**, *119*, 157701.

[134] C. Huang, S. Wu, A. M. Sanchez, J. J. P. Peters, R. Beanland, J. S. Ross, P. Rivera, W. Yao, D. H. Cobden, X. Xu, *Nat. Mater.* **2014**, *13*, 1096.

[135] A. Pospischil, M. M. Furchi, T. Mueller, *Nat. Nanotechnol.* **2014**, *9*, 257.

[136] B. W. H. Baugher, H. O. H. Churchill, Y. Yang, P. Jarillo-Herrero, *Nat. Nanotechnol.* **2014**, *9*, 262.

[137] W. Feng, W. Zheng, X. Chen, G. Liu, W. Cao, P. Hu, *Chem. Mater.* **2015**, *27*, 983.

[138] Z. Zheng, J. Yao, B. Wang, Y. Yang, G. Yang, J. Li, *ACS Appl. Mater. Interfaces* **2017**, *9*, 43830.

[139] M. S. Choi, D. Qu, D. Lee, X. Liu, K. Watanabe, T. Taniguchi, W. J. Yoo, *ACS Nano* **2014**, *8*, 9332.

[140] Y. Chen, Y. Zhang, D. Karnaushenko, L. Chen, J. Hao, F. Ding, O. G. Schmidt, *Adv. Mater.* **2017**, *29*, 1605165.

[141] J. Wang, I. Verzhbitskiy, G. Eda, *Adv. Mater.* **2018**, *30*, 1802687.

[142] Z. Wang, Q. Jingjing, X. Wang, Z. Zhang, Y. Chen, X. Huang, W. Huang, *Chem. Soc. Rev.* **2018**, *47*, 6128.

[143] N. Balakrishnan, Z. R. Kudrynskyi, M. W. Fay, G. W. Mudd, S. A. Svatek, O. Makarovsky, Z. D. Kovalyuk, L. Eaves, P. H. Beton, A. Patanè, *Adv. Opt. Mater.* **2014**, *2*, 1064.

[144] J. Hao, C. Xu, *MRS Bulletin* **2018**, 43, 965.

[145] M. C. Wong, L. Chen, G. Bai, L. B. Huang, J. Hao, *Adv. Mater.* **2017**, *29*, 1701945.

[146] M. C. Wong, L. Chen, M. K. Tsang, Y. Zhang, J. Hao, *Adv. Mater.* **2015**, *27*, 4488.

[147] Y. Zhang, W. Jie, P. Chen, W. Liu, J. Hao, *Adv. Mater.* **2018**, *30*, 1707007.

[148] C. Cui, F. Xue, W.-J. Hu, L.-J. Li, *npj 2D Mater. Appl.* **2018**, *2*, 18.

[149] Y. Bai, K. Deng, E. Kan, *Mater. Chem. Phys.* **2017**, *198*, 275.

[150] D. T. Do, S. D. Mahanti, C. W. Lai, *Sci. Rep.* **2015**, *5*, 17044.

[151] Z. Zheng, J. Yao, G. Yang, *ACS Appl. Mater. Interfaces* **2017**, *9*, 7288.

[152] D.-S. Tsai, K.-K. Liu, D.-H. Lien, M.-L. Tsai, C.-F. Kang, C.-A. Lin, L.-J. Li, J.-H. He, *ACS Nano* **2013**, *7*, 3905.

[153] M. Buscema, D. J. Groenendijk, S. I. Blanter, G. A. Steele, H. S. J. van der Zant, A. Castellanos-Gomez, *Nano Lett.* **2014**, *14*, 3347.

[154] W. Zhang, M.-H. Chiu, C.-H. Chen, W. Chen, L.-J. Li, A. T. S. Wee, *ACS Nano* **2014**, *8*, 8653.

[155] L.-H. Zeng, D. Wu, S.-H. Lin, C. Xie, H.-Y. Yuan, W. Lu, S. P. Lau, Y. Chai, L.-B. Luo, Z.-J. Li, Y. H. Tsang, *Adv. Funct. Mater.* **2019**, *29*, 1806878.

[156] L. H. Zeng, S. H. Lin, Z. J. Li, Z. X. Zhang, T. F. Zhang, C. Xie, C. H. Mak, Y. Chai, S. P. Lau, L. B. Luo, Y. H. Tsang, *Adv. Funct. Mater.* **2018**, *28*, 1705970.

[157] M. Bernardi, M. Palummo, J. C. Grossman, *Nano Lett.* **2013**, *13*, 3664.

[158] M.-L. Tsai, M.-Y. Li, J. R. D. Retamal, K.-T. Lam, Y.-C. Lin, K. Suenaga, L.-J. Chen, G. Liang, L.-J. Li, J.-H. He, *Adv. Mater.* **2017**, *29*, 1701168.

[159] Y. Tsuboi, F. Wang, D. Kozawa, K. Funahashi, S. Mouri, Y. Miyauchi, T. Takenobu, K. Matsuda, *Nanoscale* **2015**, *7*, 14476.

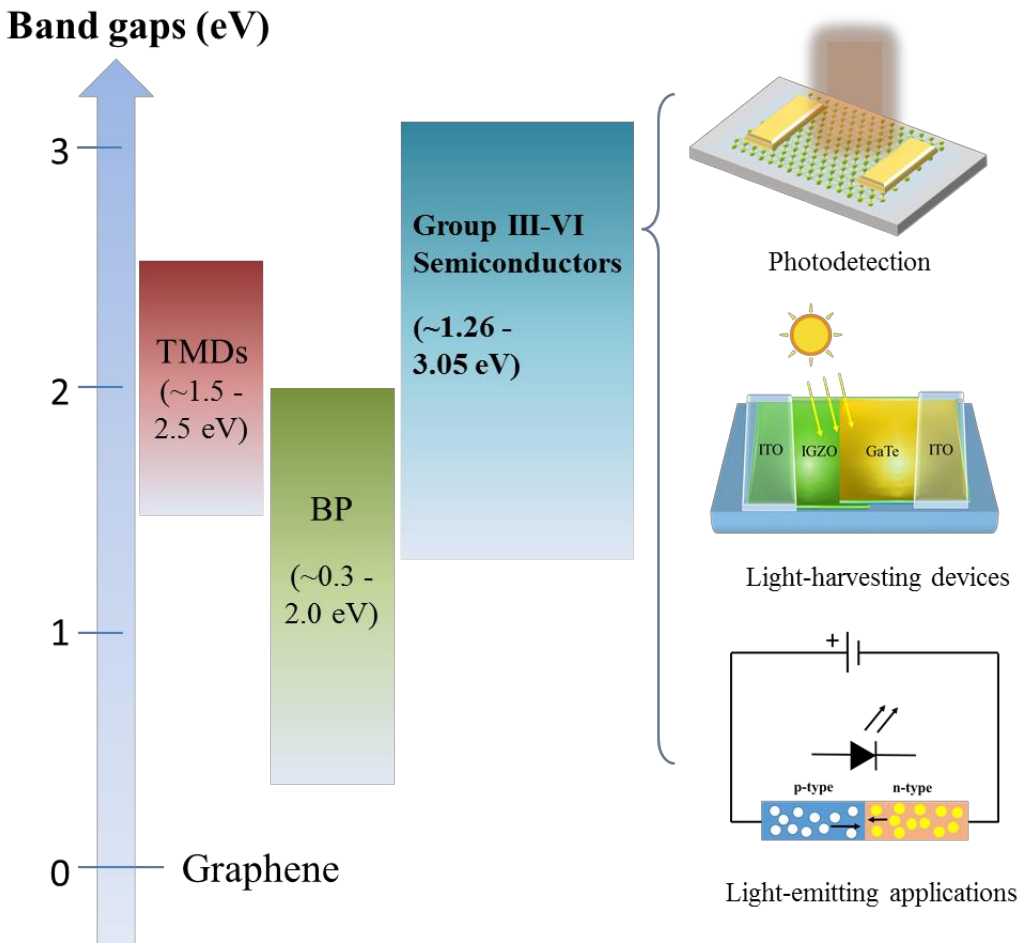

Figure 1. Optical band gaps of typical 2D layered materials (Graphene, TMDs, BP and group layered III-VI semiconductors) at room temperature and potential optoelectronic applications based on group III-VI semiconductors.

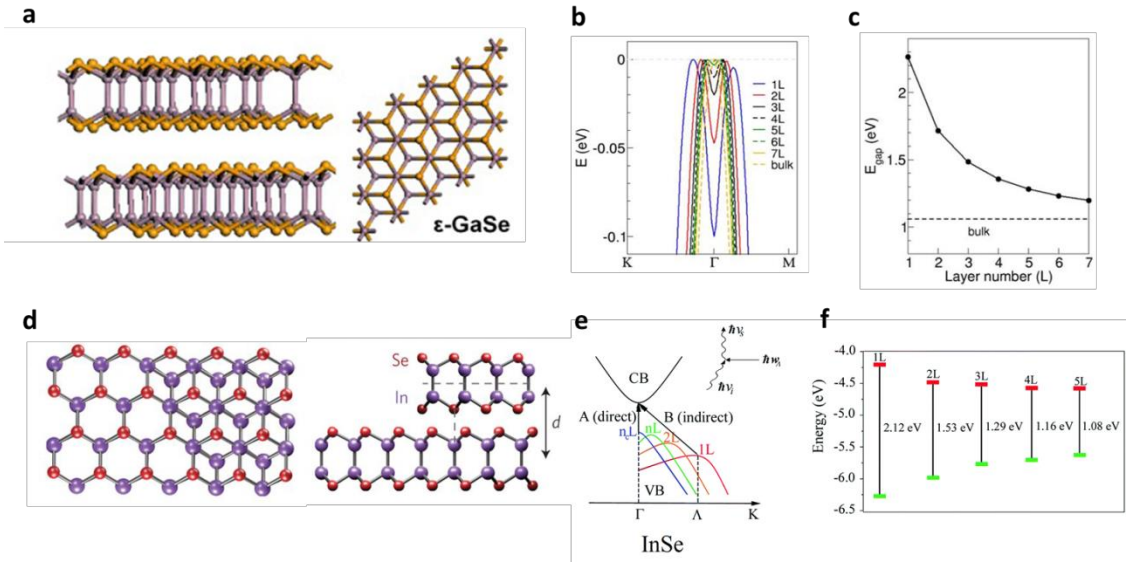

Figure 2. Crystal structure and band structure of typical 2D III-VI materials. a) Cross-sectional and top views of ε-GaSe crystal structure. Reproduced with permission.[38] Copyright 2015, Wiley-VCH. b) Energy band structures of GaSe with different layer number. c) The relationship between band gaps and layer number of GaSe nanosheets. Reproduced with permission.[37] Copyright 2014, Nature Publishing Group. d) Top and side views of mono- and bi-layer InSe. Reproduced with permission.[40] Copyright 2016, Nature Publishing Group. e) Energy band structure of different thick InSe, showing the indirect to direct band gap transition for 2D InSe. The inset image shows the photo absorption and emission process in few-layer InSe nanosheets. f) Band alignments of 2D InSe as a function of layer number. Reproduce with permission.[41] Copyright 2018, Royal Society of Chemistry.

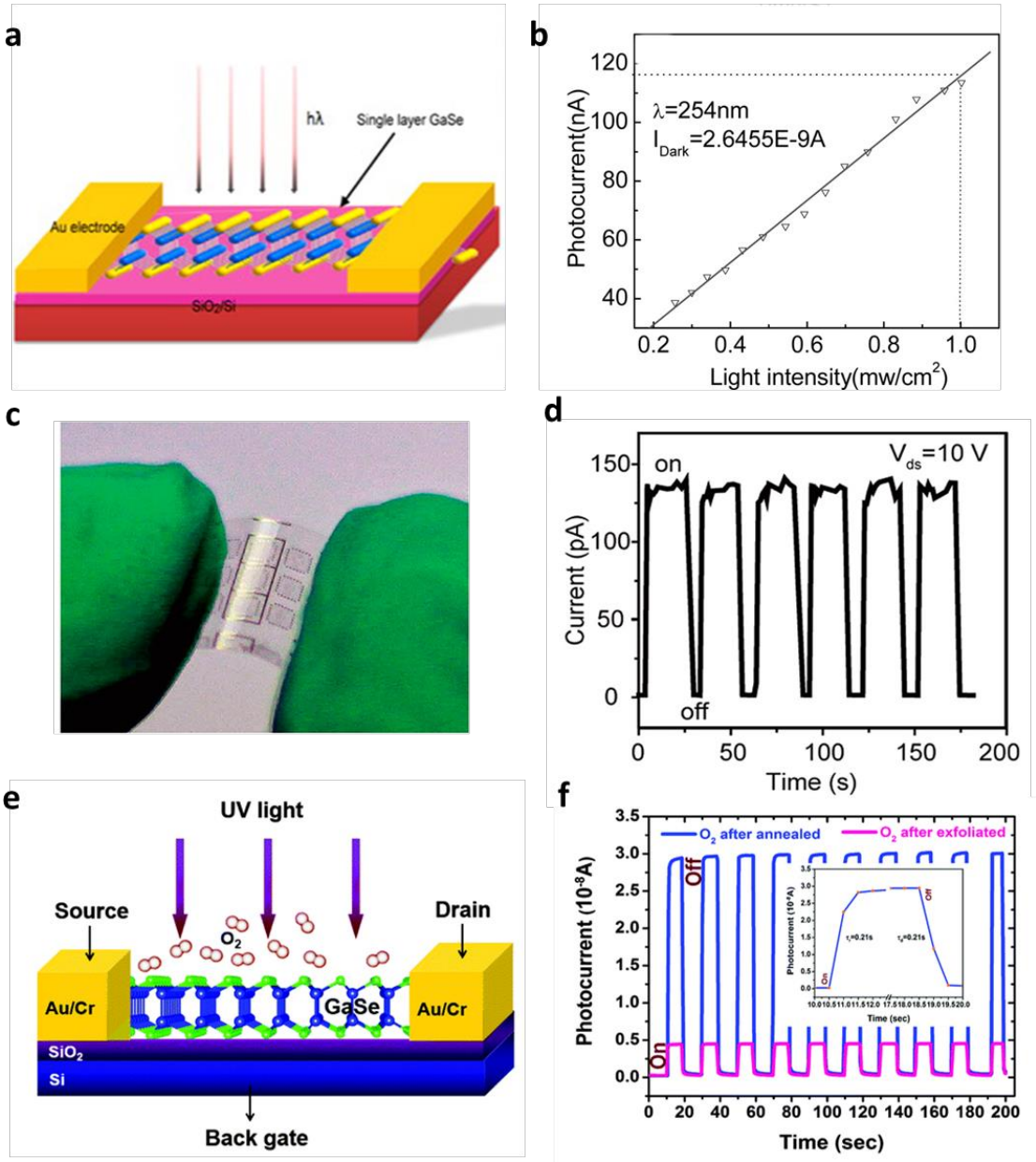

Figure 3. GaSe based photodetectors on rigid and flexible substrates, respectively. a) Schematic of photodetectors based on GaSe nanosheets. b) The illumination light intensity dependence of photocurrent. Reproduced with permission.[20] Copyright 2012, American Chemical Society. c) Optical picture of an array of GaSe photosensing devices on mica substrate with high transparency and flexibility. d) Time response of photocurrents. Reproduced with permission.[45] Copyright 2014, American Chemical Society. e)

Schematic diagram of GaSe phototransistors in the O_2 environments. f) Time response of photocurrent of the exfoliated and annealed GaSe phototransistors in the O_2 circumstance. The inset image shows one cycle of time response of photocurrent for the annealed device in O_2. Reproduced with permission.[46] Copyright 2016, Royal Society of Chemistry.

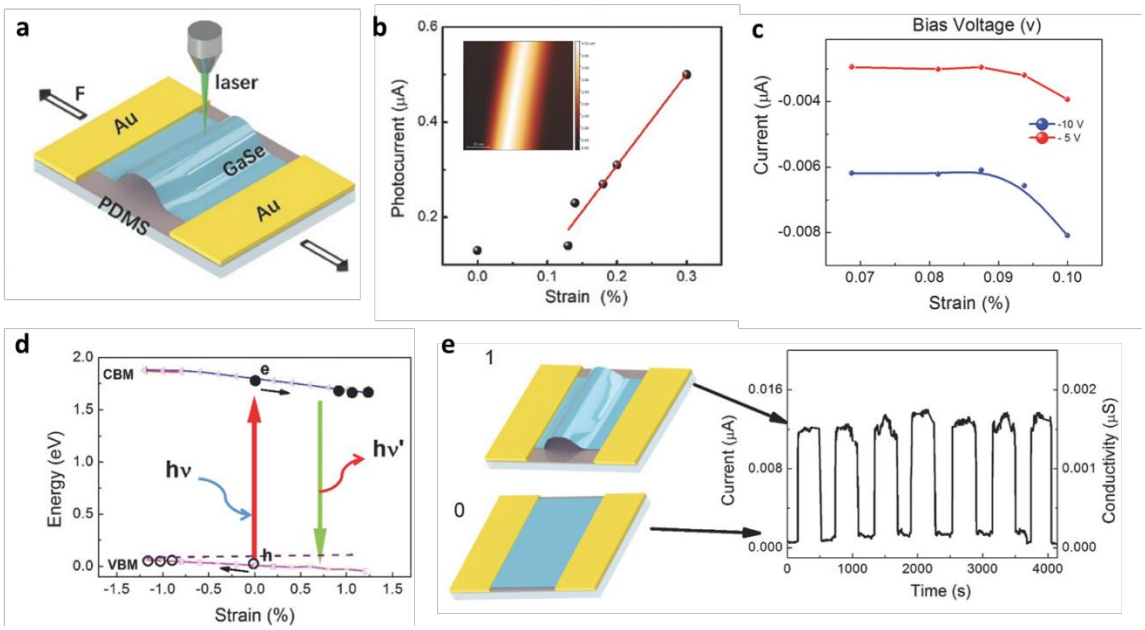

Figure 4. Piezo-phototronic responses of GaSe based flexible devices. a) Three-dimensional schematic of the GaSe photodetectors. b) The relationship between photocurrent and strain for the GaSe nanosheets when the strain is released. The inset image shows the AFM image of strained GaSe nanosheet. c) The relationship between current and strain for the laser illuminated GaSe device under different bias voltages. d) The calculated strain dependence of CBM and VBM. e) The schematics of GaSe based flexible device in unstrained and bended states. The right part of the image shows time responses of current and conductivity in different bending states of the flexible device. Reproduced with permission.[55] Copyright 2018, Wiley-VCH.

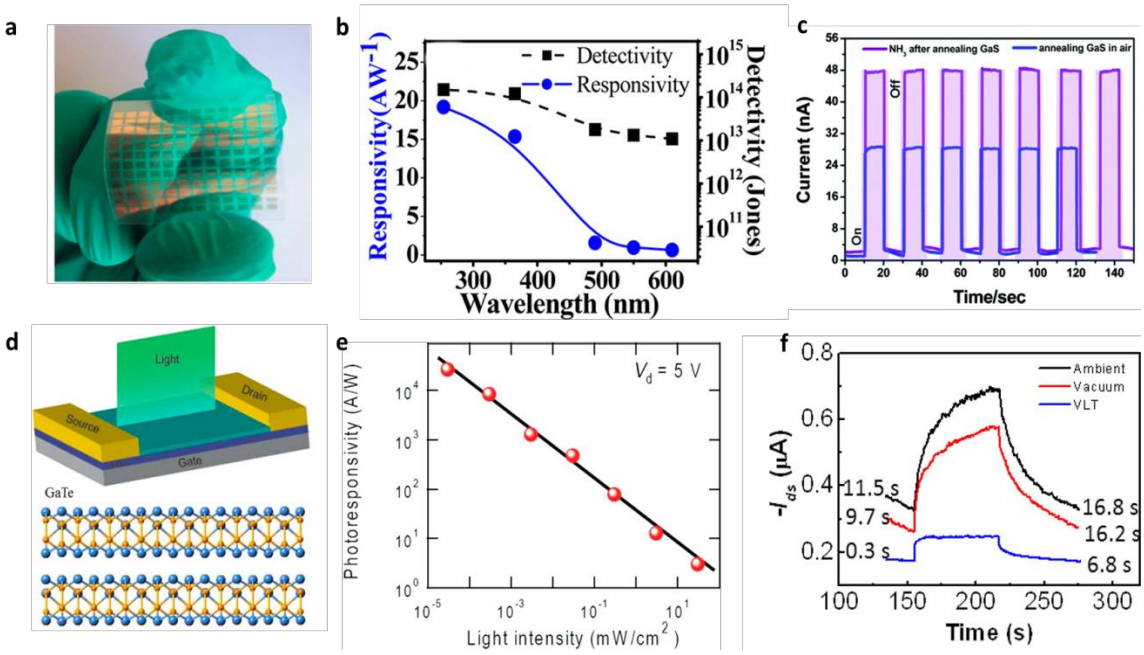

Figure 5. Optoelectronic devices based on GaS and GaTe. a) Optical picture of flexible photodetectors based on GaS nanosheets. b) The photo-responsivity and detectivity as a function of irradiation wavelength, respectively. Reproduced with permission.[27] Copyright 2013, American Chemical Society. c) Time response of the photocurrent when the light source is switched on and off in NH_3 and air environment, respectively. Reproduced with permission.[56] Copyright 2014, Royal Society of Chemistry. d) The side view of GaTe crystal structure and schematic of GaTe photodetector. e) The photo-responsivity as a function of illuminated light intensity. Reproduced with permission.[21] Copyright 2014, American Chemical Society. f) Time response of the photocurrent when the laser is switched on and off under environments of ambient, vacuum and VLT, respectively. Reproduced with permission.[59] Copyright 2014, American Chemical Society.

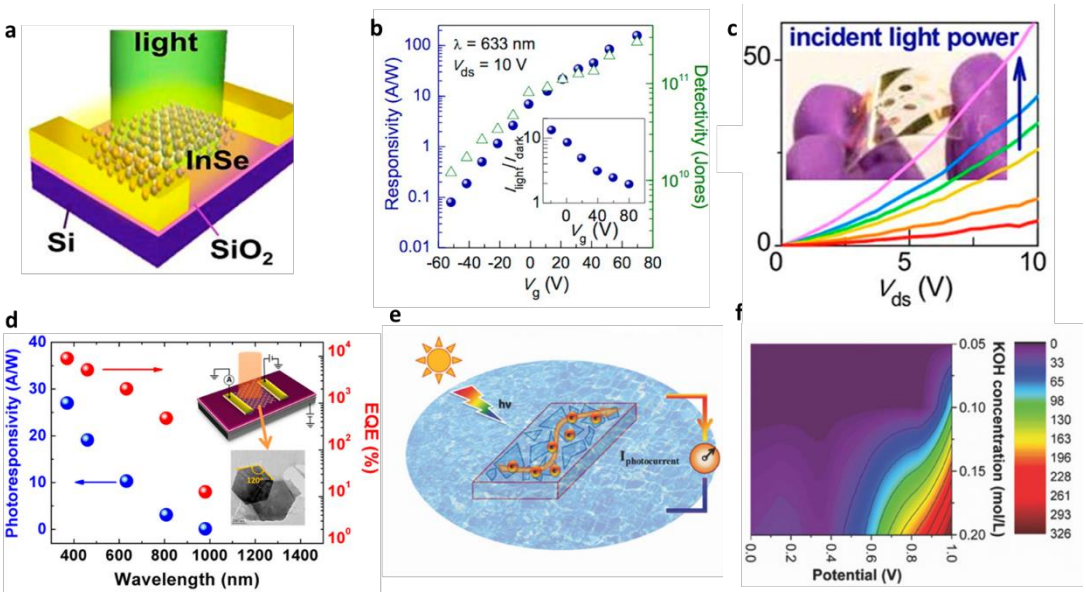

Figure 6. Characterization of photo response of InSe based photo-sensing devices. a) Schematic drawing of InSe based photodetector. b) The gate bias dependence of photo responsivity and detectivity. The inset image shows the ratio of I_{light} and I_{dark} as a function of gate bias. c) The photocurrent of flexible InSe photodetector as a function of drain-source bias under different light intensity. The inset image shows the digital picture of bended InSe device on PET substrates. Reproduced with permission.[30] Copyright 2014, American Chemical Society. d) The photo-responsivity and EQE of wafer-scale InSe phototransistors as a function of wavelength, respectively. The right upper inset image shows the schematic image of the InSe device. The right lower inset image shows the TEM image of InSe nanosheets (Scale bar: 200 nm). Reproduced with permission.[42] Copyright 2017, American Chemical Society. e) The schematic image of the InSe photo-electrochemical photodetector. f) Photocurrents of InSe based photodetectors in response to both KOH concentration and external potential. Reproduced with permission.[70] Copyright 2018, Wiley-VCH.

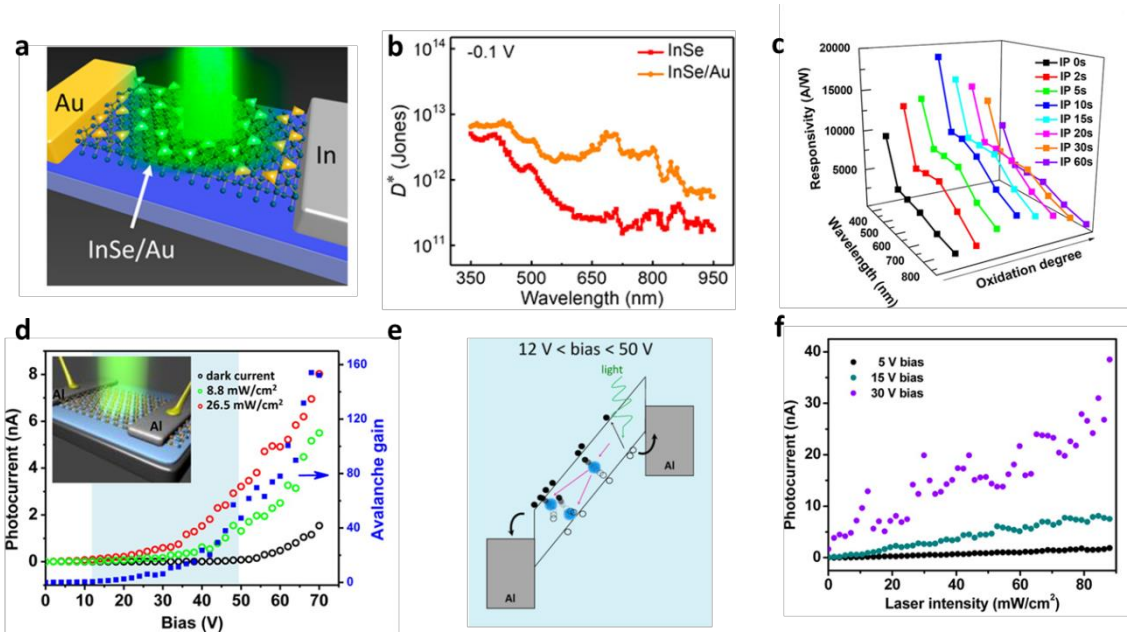

Figure 7. The enhancement of performances of InSe based photo sensing devices. a) 3D schematic image of InSe self-powered photodetector covered with the Au triangular nanoarrays. b) The curves of detectivities of InSe and InSe/Au photodetectors versus wavelength, respectively. Reproduced with permission.[76] Copyright 2018, American Chemical Society. c) The photoresponsivity of oxygen plasma treated InSe phototransistor as a function of both wavelength and oxidation degree. Reproduced with permission.[77] Copyright 2017, American Chemical Society. d) The photocurrents and avalanche gain of InSe based photodetectors under different illumination intensities as a function of gate bias. The inset image shows the schematic of avalanche photodetector based on monolayer InSe. e) The illustration of working principle of the InSe based avalanche photodetector under the biases of 12 to 50 V. f) The relationship between the photocurrents and the illumination laser intensity upon different gate biases (5 V, 15 V, 30 V). Reproduced with permission.[79] Copyright 2015, American Chemical Society.

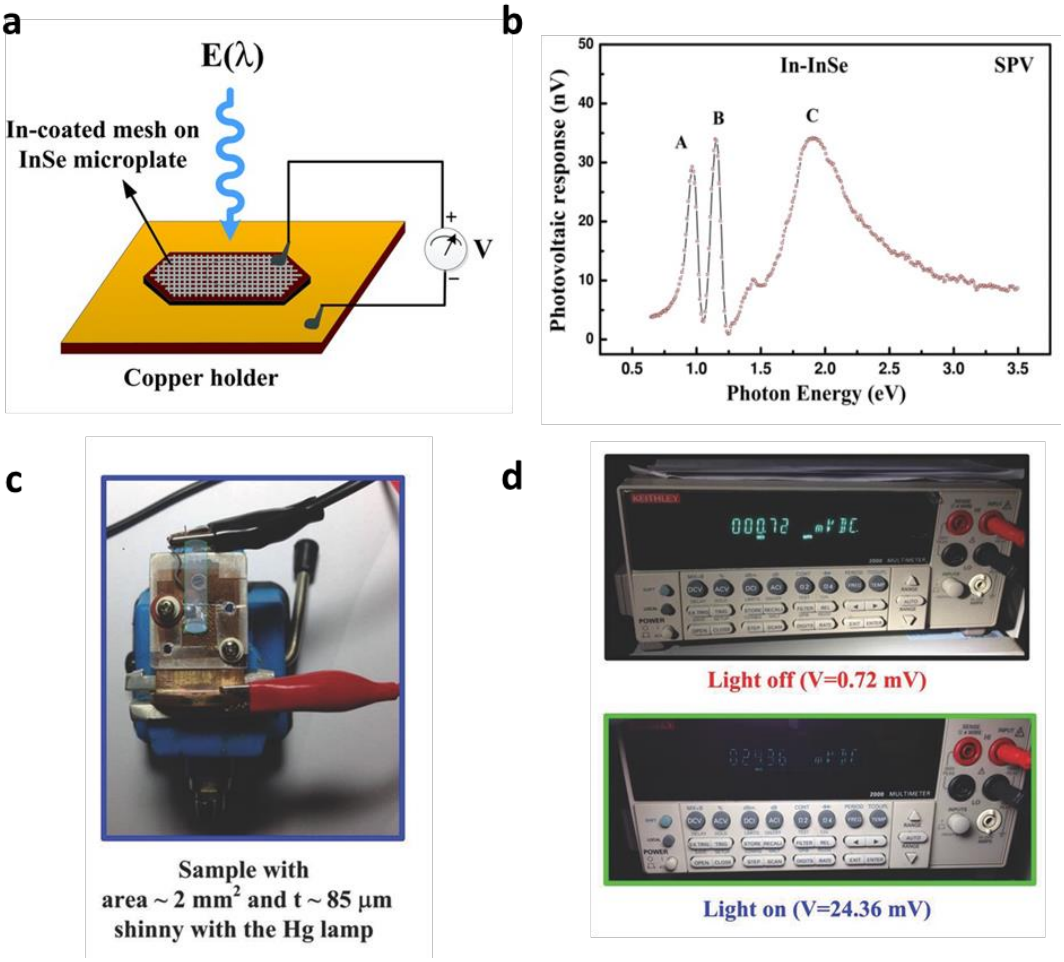

Figure 8. Characterization of Schottky-type solar cell based on InSe. a) SPV measurement setup of InSe solar cell. b) The photovoltaic effect as a function of illumination photon energy for In-InSe solar cell. c) Optical picture of Schottky solar cell based on InSe and measurement setup. d) The demonstration of output photovoltaic effect of InSe solar cell. Reproduced with permission.[78] Copyright 2015, Wiley-VCH.

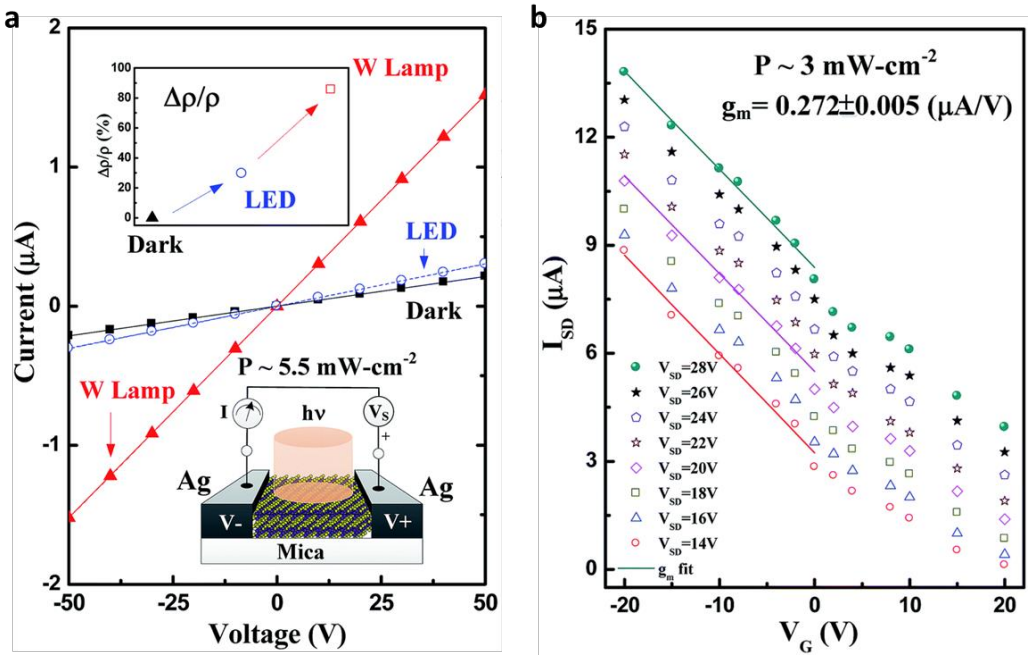

Figure 9. Characterization of photo sensing properties of a new prototype Photo-MESFET based on InS. a) I-V characteristics of InS device illuminated by different light sources. The upper inset image shows Δρ/ρ for different illumination conditions. The lower inset image presents two-dimensional schematic of the InS based Photo-MESFET and the measurement setup. b) The I_{SD} as a function of V_G at different V_{SD} of the InS Photo-MESFET. Reproduced with permission.[81] Copyright 2016, Royal Society of Chemistry.

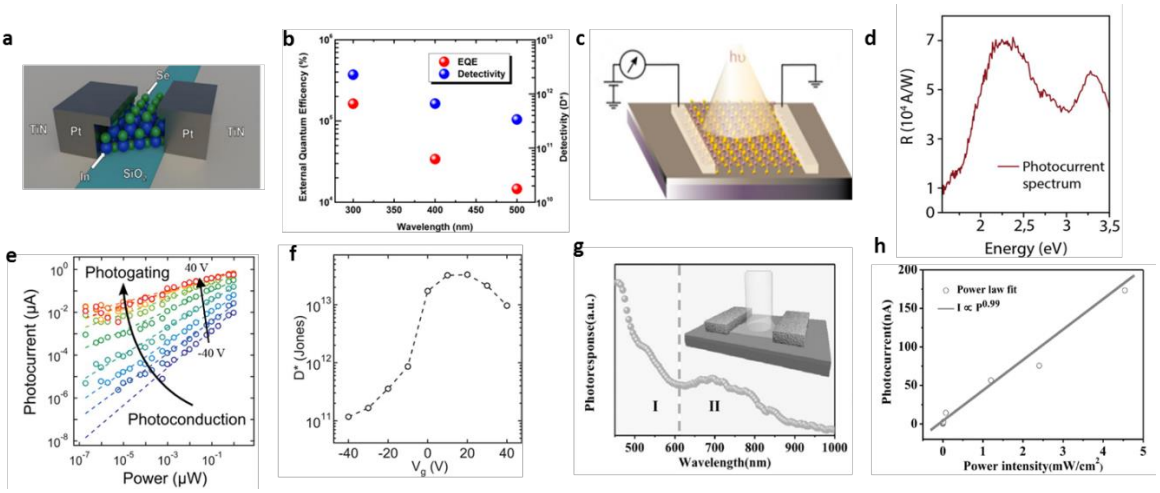

Figure 10. Optoelectronic devices based on 2D layered In_2S_3 and In_2Se_3. a) Schematic image of photodetector based on α-In_2Se_3 nanosheet. b) EQE and detectivity as a function of illumination wavelength, respectively. Reproduced with permission.[91] Copyright 2014, American Chemical Society. c) Schematic of colloidal monolayer β-In_2Se_3 based photodetector. d) The photoresponsivity as a function of photon energy for β-In_2Se_3 based photodetector. Reproduced with permission.[92] Copyright 2017, American Chemical Society. e) The photocurrent of In_2Se_3 phototransistors as a function of illumination power under different gate biases. f) The curve of inferred detectivity versus gate biases. Reproduced with permission.[23] Copyright 2015, American Chemical Society. g) The wavelength dependent photoresponses of In_2S_3 photodetector. The inset image shows the schematic of the device. h) The photocurrent of In_2S_3 phtodetector as a function of incident light intensity. Reproduced with permission.[24] Copyright 2017, Wiley VCH.

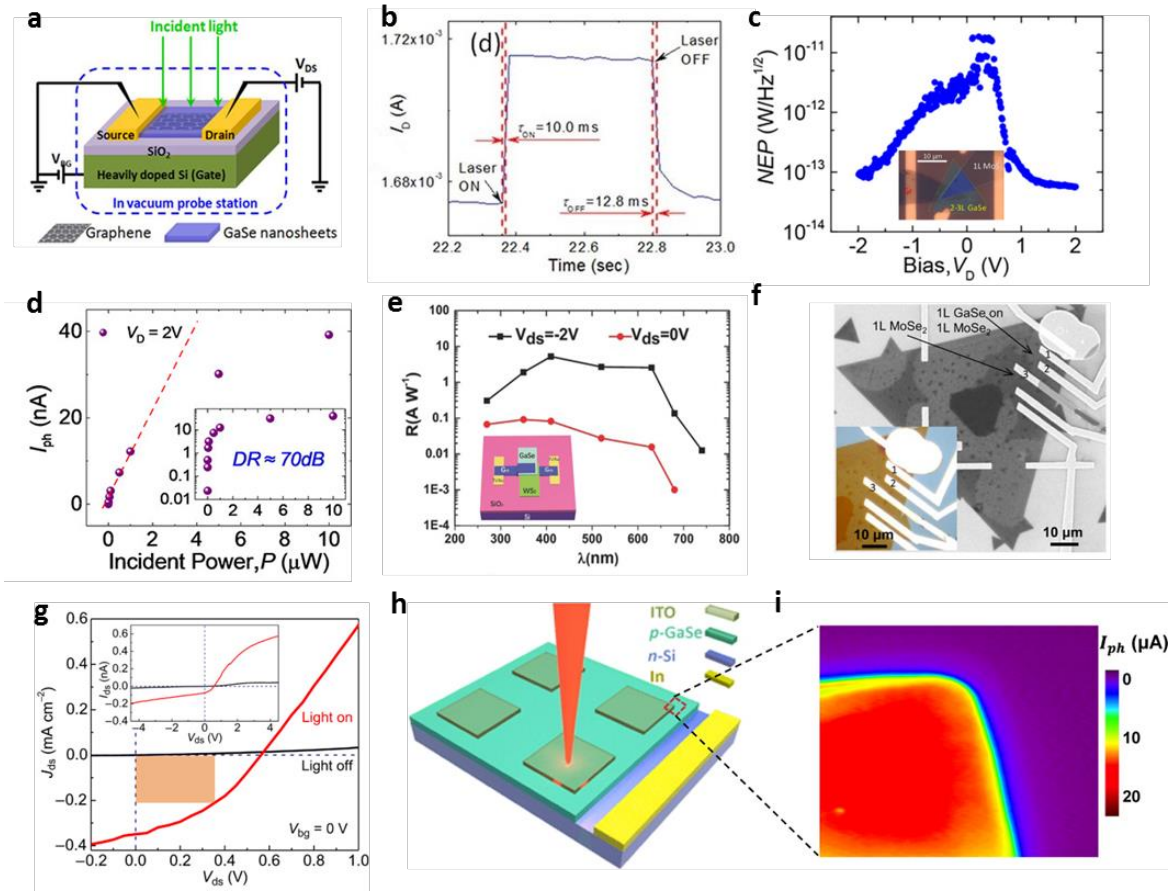

Figure 11. Optoelectronic devices based on 2D GaSe heterostructures. a) 3D schematic image of photodetector based on graphene/GaSe heterostructure and corresponding measurement setup. b) Current response of graphene/GaSe photodetector to one pulse of 532 nm laser at zero gate bias. Reproduced with permission.[101] Copyright 2016, Nature Publishing Group. c) Noise equivalent power (NEP) of photodiode based on GaSe/MoS_2 heterostructure. The inset image shows the optical images of device (Scale bar: 10 μm). d) The photocurrent as a function of increasing incident light power. The inset image shows the logarithmic scale of photocurrent versus light power. Reproduced with permission.[105] Copyright 2018, American Chemical Society. e) The relationship between photoresponsivity (R) and the wavelength of incident light (λ) at different drain-source biases. The inset image shows the schematic picture of device based on graphene

sandwiched GaSe/WS_2 heterostructure. Reproduced with permission.[103] Copyright 2018, Wiley VCH. f) SEM image of optoelectronic devices based on GaSe/$MoSe_2$ heterostructure. The inset image presents the corresponding optical image. g) The curves of drain-source current density (J_{ds}) versus drain-source bias (V_{ds}) upon on and off states for the white light illuminating on the heterojunction, revealing observation of the photovoltaic effect of the device. The P_{max} is indicated by the square with orange color. The inset image shows the I_{ds}-V_{ds} characterization with a larger scale. Reproduced with permission.[102] Copyright 2016, AAAS. h) Schematic image of photodiode based on the arrayed heterostructure of ITO/p-GaSe/n-Si/In. i) The spatially resolved photocurrent mapping for the corner of the device, showing uniformly distributed photocurrent in the junction area. Reproduced with permission.[110] Copyright 2015, American Chemical Society.

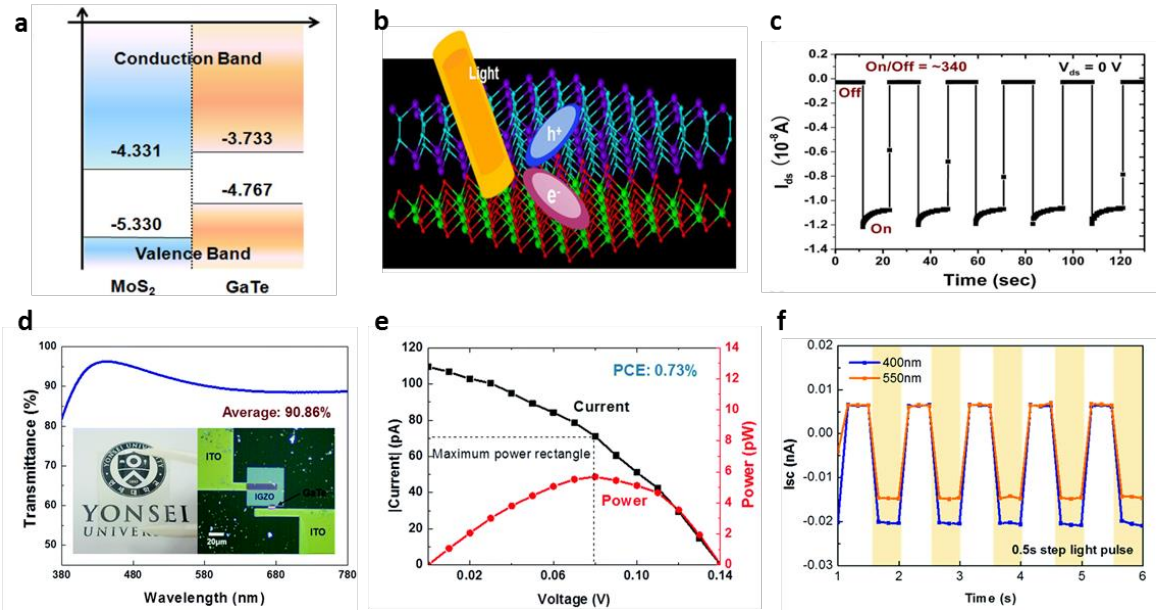

Figure 12. Optoelectronic devices fabricated by GaTe based heterostructures. a) Schematic of theoretically obtained band diagram of the GaTe/MoS_2 heterostructure, indicating formation of type-II heterojunction. b) The schematic drawing to show the separation process of photoexcitons. c) Time resolved photoresponse of photodetectors based on GaTe/MoS_2 heterostructure under zero drain bias. Reproduced with permission.[35] Copyright 2016, American Chemical Society. d) The curve of transmittance (%) versus wavelength for the GaTe/IGZO solar cell. The inset exhibits the optical pictures and microscope image of the device. e) The relationship between current /generated power of the device and bias voltage. f) Time resolved short-circuit current of the GaTe/IGZO solar cell in response to the dynamic light with different wavelength (400 and 500 nm). Reproduced with permission.[117] Copyright 2017, Royal Society of Chemistry.

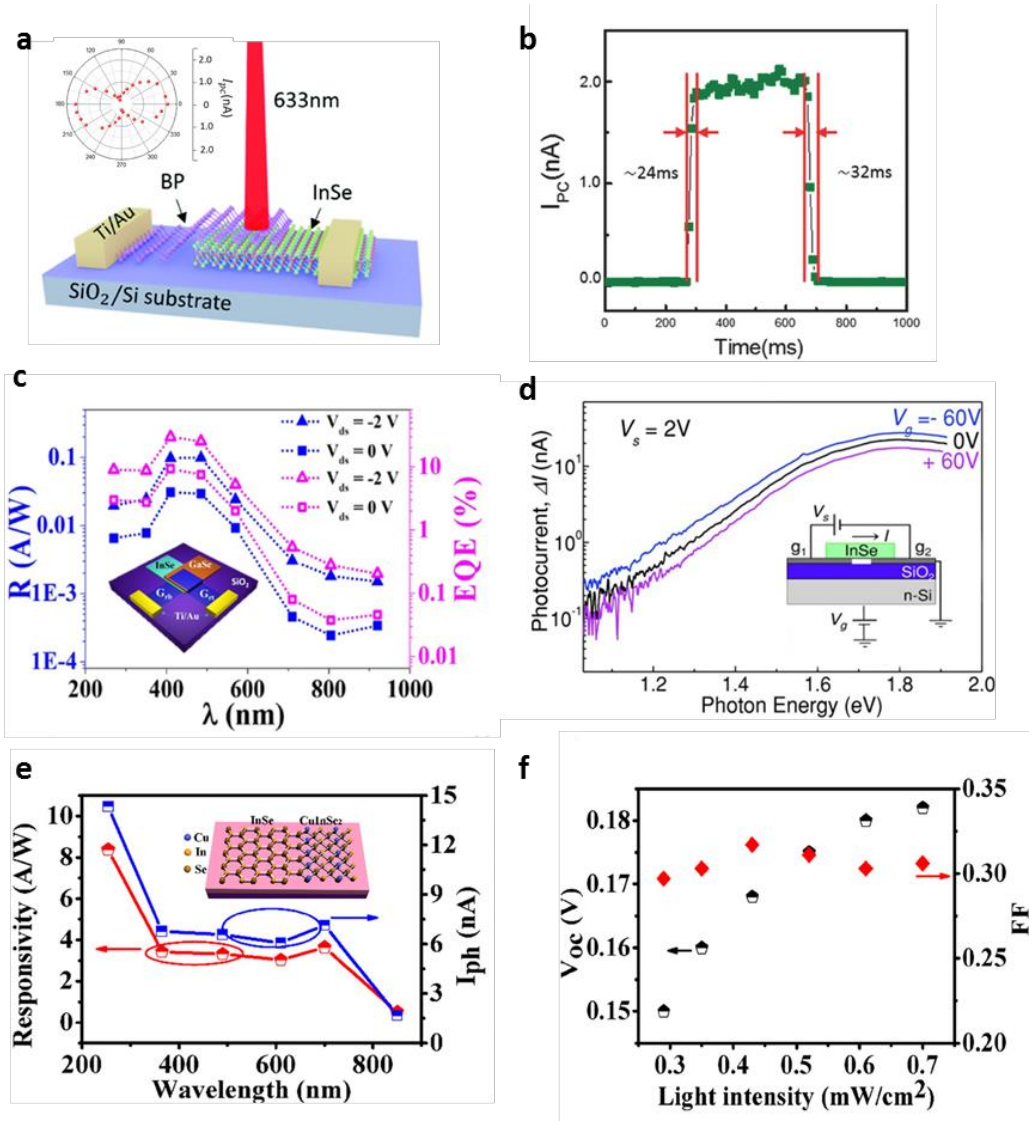

Figure 13. Demonstration of optoelectronic devices based on InSe 2D vdWs heterostructures. a) Schematic illustration of photodetectors based on BP/InSe heterostructure. The left corner inset shows the polar plot of the angle resolved polarized photocurrent response under zero bias voltage. b) Time dependent photoresponse of BP/InSe photodetector, showing rise and fall response time of 24 and 32 ms, respectively. Reproduced with permission.[34] Copyright 2018, Wiley VCH. c) The curves of photoresponsivity (R) and EQE (%) versus wavelength of illumination light at different drain-source biases of GaSe/InSe photodiode at room temperature. The inset image shows

the schematic image of the photodiode based on GaSe/InSe heterojunction. Reproduced with permission.[120] Copyright 2017, IOP Publishing Ltd. d) The photocurrent of photodetector based on InSe/graphene heterostructure as a function of incident photon energy under different gate biases. The inset image shows the schematic diagram of the device. Reproduced with permission.[122] Copyright 2015, Wiley VCH. e) Photoresponsivity and photocurrent (I_{ph}) of photodetector based on InSe-$CuInSe_2$ lateral heterojunction versus wavelengths of illumination light at drain-source bias of -10 V. The inset image shows the schematic image of InSe-$CuInSe_2$ lateral heterostructure. f) Characterization of InSe/$CuInSe_2$ based solar cell, exhibiting the light intensity dependent open-circuit voltage and fill factor (FF), respectively. Reproduced with permission.[131] Copyright 2015, American Chemical Society.

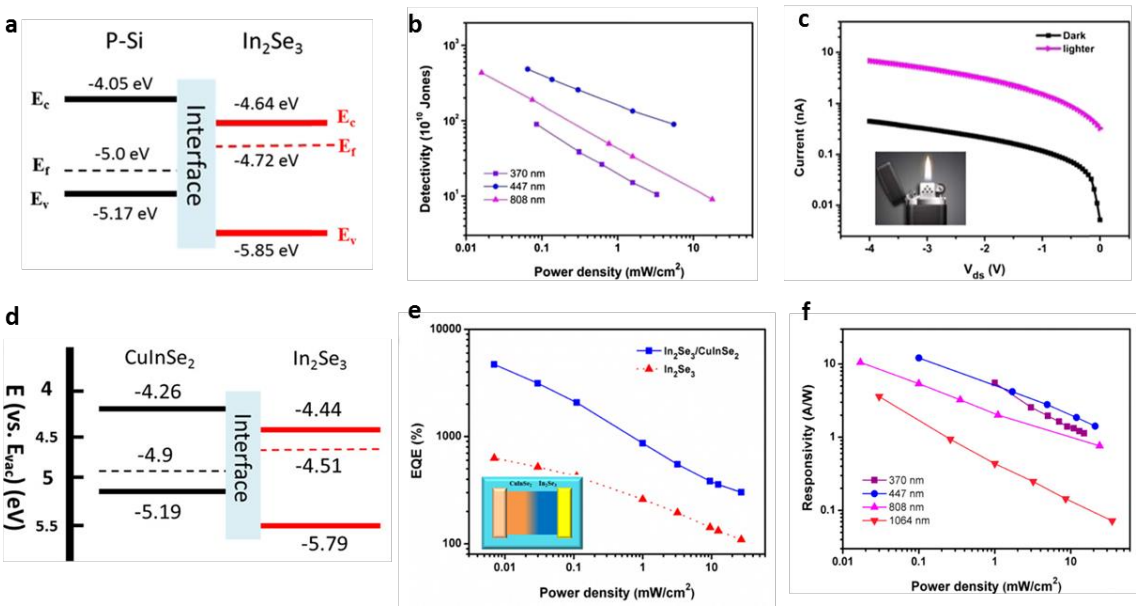

Figure 14. Characterization of photodetectors based on In_2Se_3 heterostructures. a) Schematic diagram of band alignment of β-In_2Se_3/Si heterojunction. b) Detectivity as a function of illumination power density of the β-In_2Se_3/Si photodetector. c) Characterization of sensing ability of the device for weak signal from a lighter. The inset image shows the optical photograph of the lighter. Reproduced with permission.[132] Copyright 2017, American Chemical Society. d) Schematic diagram of band alignment of lateral β-In_2Se_3-$CuInSe_3$ heterojunction. e) EQE (%) of the β-In_2Se_3-$CuInSe_3$ photodetector as a function of incident power density. The inset image shows the schematic diagram of the device. f) The photoresponsivity of the device as a function of incident power density for different illumination wavelength, covering from 370 nm to 1064 nm. Reproduced with permission.[144] Copyright 2017, American Chemical Society.

Table 1. Band gaps of bulk and 2D forms of III-VI semiconductors at room temperature.

	Direct band gaps (eV)	Indirect band gap (eV)	Nature of band gap	Refs
Bulk GaS	3.05	2.59	Indirect	[28]
Monolayer GaS	-	3.22	Indirect	[149]
Bulk GaSe	2.13	2.11	Indirect	[21]
Few-layer GaSe	2.082	2.031	Indirect	[40]
Bulk GaTe	1.7	-	Direct	[22]
Monolayer GaTe (Theoretical)	1.4	-	Indirect	[150]
Bulk InSe	1.25	-	Direct	[29]
Monolayer InSe	-	2.1	Indirect	[29]
Bulk In_2S_3	1.9	-	Direct	[25]
Few-layer In_2S_3	2.3	-	Direct	[25]
Bulk In_2Se_3	1.3	-	Direct	[95]
Monolayer In_2Se_3	1.55	-	Direct	[89]

Table 2. FOM of photo-sensing devices based on layered group IIIA chalcogenides and some other typical 2D materials

Materials	Measurement conditions		Spectral range	R (AW^{-1})	D*(Jones)	Response time (ms)	Refs
	λ (nm)	V_{ds} (V)					
GaS	254	2	254-610	19.2	10^{14}	≤30	[28]
Exfoliated GaSe	254	5	254-610	2.8	-	20	[21]
PLD-GaSe	700	2	240-1000	0.4	-	-	[47]
GaTe	532	5	-	10^4	-	6	[22]
CVD-GaTe	473	5	-	0.03	-	54	[62]
Exfoliated InSe	633	10	450-785	7	$\sim10^{11}$	40	[31]
PLD-InSe	370	1	370-980	27	-	500	[44]
CVD-In_2S_3	450	1	400-1000	137	4.74×10^{10}	6	[25]
Exfoliated α-In_2Se_3	300	5	300-1100	395	2.26×10^{12}	18	[95]
PLD-In_2Se_3	532	5	254-1064	20.5	6.02×10^{11}	24.6	[94]
Graphene/ GaSe	532	1	-	3.5×10^5	$\sim10^{10}$	10	[107]
GaSe/WS_2	410	2	270-740	149	4.3×10^{12}	0.037	[109]
GaTe/MoS_2	633	0	-	1.365	-	≤10	[37]

BP/InSe	455	0.5	455-950	0.0117	-	24	[36]
GaSe/InSe	410	2	270-920	350	3.7×10^{12}	0.002	[126]
InSe/ graphene	633	2	-	4×10^{3}	10^{10}	1	[128]
InSe-$CuInSe_2$	254	10	254-850	8.4	-	-	[137]
β-In_2Se_3/Si	532	4	370-808	5.9	4.9×10^{12}	8.3	[138]
In_2Se_3-$CuInSe_2$	532	2	370-1550	20.1	-	8.3	[151]
MoS_2	670	1	-	7.5×10^{-3}	-	50	[67]
CVD-MoS_2	532	10	400-800	0.57	10^{10}	0.07	[152]
BP	640	0.2	400-940	4.8×10^{-3}	-	1	[153]
WSe_2	650	2	500-900	1.8×10^{5}	10^{14}	5×10^{3}	[154]
$PdSe_2$/Si	780	0	-	0.3	10^{13}	0.038	[155]
$PtSe_2$/GaAs	808	0	650-810	0.262	2.52×10^{12}	0.005	[156]

Table 3. FOM of photovoltaic devices based on layered group IIIA chalcogenides and some other typical 2D materials

Materials	Thickness (nm)	J_{SC} (mA/cm^2)	V_{OC} (V)	FF	PCE (%)	Refs.
GaSe/$MoSe_2$	~1.8	0.35	0.57	0.38	0.12	[108]
GaTe/InGaZnO	~120	0.63	0.14	0.37	0.73	[123]
InSe-$CuInSe_2$	20-50	-	0.18	0.3	3.5	[137]
Graphene/MoS_2	0.9	4.3-4.5	0.1-0.5	0.3-0.6	0.1-1	[157]
Phosphorene/MoS_2	~12	-	0.1~0.3	0.5	0.3	[129]
WSe_2/MoS_2	~1	-	0.39	0.3701	2.56	[158]
Graphene/MoS_2/ n-Si	20	13.1	0.41	0.25	1.35	[159]